Constraining the Intracontinental Tectonics of the SW Central Asian Orogenic Belt by the Early Permian Paleomagnetic Pole for the Turfan-Hami Block

Xin Zhu, Bo Wang, Yan Chen, Hongsheng Liu

JGR Solid Earth

RESEARCH ARTICLE
10.1029/2019JB017680

Key Points:
- The first Early Permian paleomagnetic pole for the Turfan-Hami basin is obtained
- Large-magnitude strike-slip displacement along megashear zones is confirmed as dominant intracontinental tectonics in the SW CAOB
- An Early Permian intra-arc basin of ~530 km width is proposed to exist in the Bogda belt, between the Turpan-Hami and South Junggar blocks

Supporting Information:
- Supporting Information S1
- Table S1
- Table S2
- Table S3
- Table S4

Correspondence to:
B. Wang,
bwang@nju.edu.cn;
burh_cw@yahoo.com

Citation:
Zhu, X., Wang, B., Chen, Y., & Liu, H. (2019). Constraining the Intracontinental Tectonics of the SW Central Asian Orogenic Belt by the Early Permian Paleomagnetic Pole for the Turfan-Hami Block. *Journal of Geophysical Research: Solid Earth*, *124*. https://doi.org/10.1029/2019JB017680

Received 12 MAR 2019
Accepted 14 NOV 2019
Accepted article online 21 NOV 2019

Constraining the Intracontinental Tectonics of the SW Central Asian Orogenic Belt by the Early Permian Paleomagnetic Pole for the Turfan-Hami Block

Xin Zhu[1,2], Bo Wang[1], Yan Chen[2], and Hongsheng Liu[1,3]

[1]State Key Laboratory for Mineral Deposits Research, School of Earth Sciences and Engineering, Nanjing University, Nanjing, China, [2]Univ. Orléans, CNRS, BRGM, ISTO, UMR 7327, F-45071, Orléans, France, [3]School of Geoscience and Info Physics, Central South University, Changsha, China

Abstract In order to better understand the kinematics and geodynamics of the late Paleozoic to early Mesozoic transition from accretionary to intracontinental tectonics in the southwest Central Asian Orogenic Belt, we performed a paleomagnetic study on Lower Permian strata in the Turpan-Hami Basin, NW China. Magnetite and hematite are shown to be the principal magnetic remanence carriers. A typical sedimentary fabric that has not been modified by postdepositional deformation is recognized via magnetic fabric study. Stable characteristic remanent magnetizations, all of reverse magnetic polarity, are revealed by step demagnetizations. Remanence age is determined to be of Early Permian affinity, based on a fold test, remanence behavior of minerals, and geochronologic data. With inclination shallowing corrections, the first Early Permian paleomagnetic pole for the Turpan-Hami Block is acquired as $\lambda = 75.7°$N, $\varphi = 276.3°$E, $A_{95} = 5.7°$, and $N = 10$ sites. Comparisons of this new pole with published ones from neighboring cratonic blocks provide kinematic constraints on the tectonic transition and subsequent intracontinental tectonics of this region. The Turpan-Hami and Yili blocks have kept their relative positions since the Early Permian. Significant latitudinal movement of $14.7° \pm 7.2°$ occurred between the Turpan-Hami and South Junggar blocks and could be mainly accommodated by late Paleozoic crustal shortening of at least ~530 km across an intra-arc basin in the Bogda belt. The Turpan-Hami Block has experienced large-magnitude relative rotations of $-41.1° \pm 7.1°$ and $21.2° \pm 9.4°$ with respect to Tarim and South Junggar since the Early Permian, respectively, corresponding to dominant intracontinental tectonics characterized by large-magnitude strike-slip displacements along megashear zones.

1. Introduction

Kinematics along the major boundaries between microcontinental blocks and/or terranes is the key to decipher the geodynamic evolution of orogenic belts and to understand mechanisms of transition from subduction-accretion to intracontinental tectonics. Plate boundaries in orogenic belts usually experience long and multistaged deformation, and geodynamic reconstruction using geologic records often becomes complicated and controversial. Paleomagnetism is a workable method to study these processes, as it can provide quantitative, large-scale constraints on the kinematics of blocks, including paleolatitudinal translation and vertical-axis rotation (Butler, 1992).

Located between the Siberia Craton to the north and the Karakorum, Tarim, and North China cratons to the south, the Central Asian Orogenic Belt (CAOB; Figure 1a; Jahn, 2004) or the Altaïds (Sengör et al., 1993), extending from the Urals in the west to the Pacific Ocean in the east, is the largest Phanerozoic accretion/collisional orogenic system on the Earth. It is widely accepted that the CAOB was assembled by different microcontinents, island arcs, seamounts, and accretionary wedges through Paleozoic successive accretion and collision (e.g., Wilhem et al., 2012; Windley et al., 2007). The CAOB subsequently experienced significant intracontinental reworking dominated by the late Paleozoic to Mesozoic large-scale strike-slip faulting (e.g., Allen et al., 1993; Laurent-Charvet et al., 2003; Wang et al., 2007, 2009). Finally, it underwent Cenozoic crustal shortening and uplift in response to the India-Eurasia collision (e.g., Avouac et al., 1993; Chen et al., 1992; Molnar & Tapponnier, 1975). Thus, it is an optimal region for investigating the transition from accretionary to intracontinental tectonics.

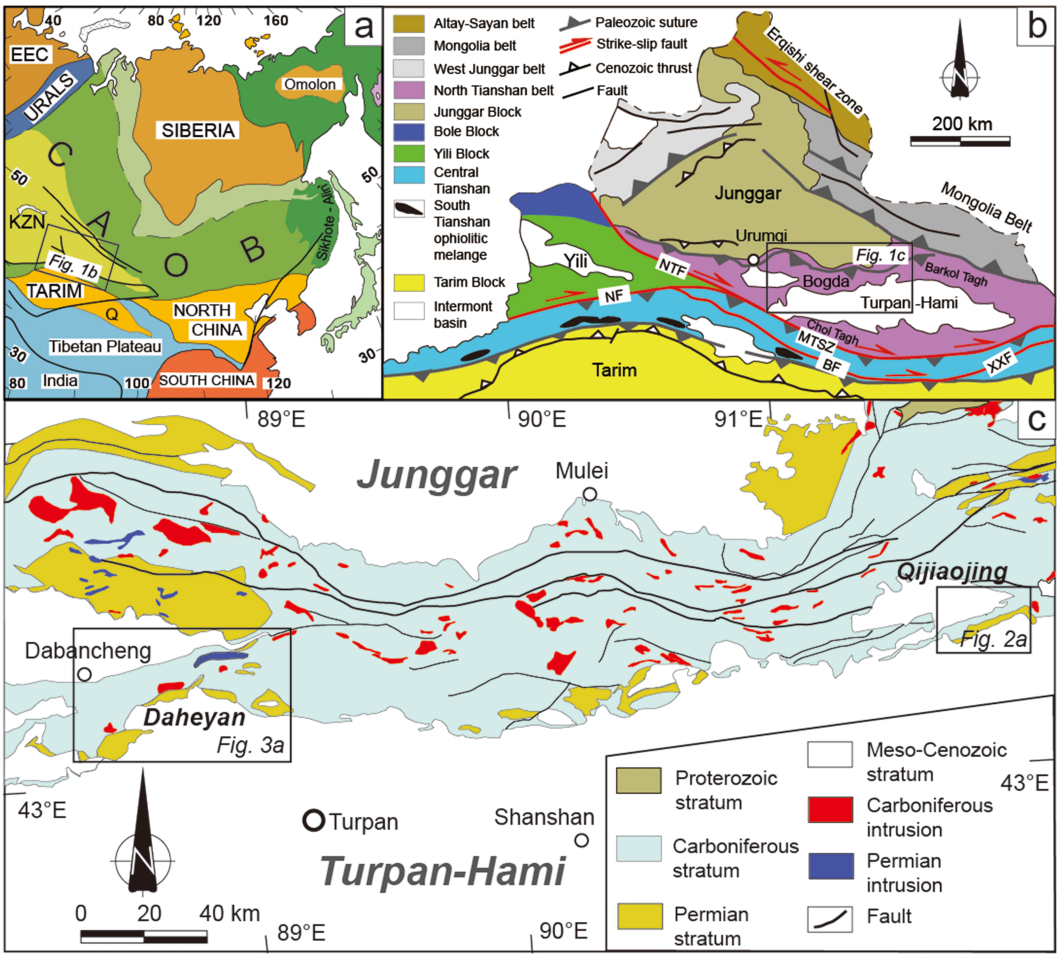

Figure 1. (a) Simplified tectonic division of the eastern Asia showing the location of the central Asian Orogenic Belt (CAOB) and its surrounding blocks (after Jahn, 2004). (b) Simplified tectonic division of the Chinese Tianshan area, SW CAOB (after Wang et al., 2007). (c) Simplified geologic map of the Bogda Belt, northern margin of the Turpan-Hami basin (modified from XGSC, 2007 and Wali et al., 2018). EEC = East European Craton; KZN = Kazakhstan; Q = Qaidam; BF = Baluntai fault; MTSZ = main Tianshan shear zone; NF = Nalati fault; NTF = North Tianshan fault; XXF = Xingxingxia fault.

The mechanism of tectonic transition from subduction-accretion to postcollisional intracontinental deformation is the focus of debate in the geodynamic reconstruction of the CAOB. Several hypotheses, including oblique convergence (Choulet et al., 2012; Wang et al., 2009), slab break-off (Ma et al., 2015; Yuan et al., 2010), and extrusion tectonics (Wang et al., 2007; Wang et al., 2008), have been proposed to interpret the end Paleozoic to early Mesozoic tectonic transition. Furthermore, different tectonic settings were also suggested for the Early Permian tectonic and magmatic environment, such as ridge subduction (Geng et al., 2009) and super mantle plume-related large igneous province (Su et al., 2011; Xia et al., 2008), which are mostly based on geochemical studies on magmatic rocks.

Recently, several paleomagnetic studies were conducted in the SW CAOB and provided important constraints for the relative paleogeographic positions of the Yili and South Junggar blocks (Choulet et al., 2011; Choulet et al., 2013; Wang et al., 2007; Zhu et al., 2018). However, the paleomagnetic data are still scarce in the Turpan-Hami Block (Figure 1b; Cogné et al., 1995; Huang et al., 2004, Huang et al., 2004) and remain completely lacking for the Paleozoic. Considering that the Turpan-Hami Block played a pivotal role in the late Paleozoic accretion and the subsequent intracontinental tectonics of the CAOB (Chen et al., 2015; Greene et al., 2001, 2005; Wali et al., 2018; Wartes et al., 2002), Early Permian paleomagnetic data from this area could be of great importance. Therefore, we performed a paleomagnetic study on Early Permian rocks from the Turpan-Hami Basin.

2. Geological Background and Paleomagnetic Sampling

The Tianshan orogenic belt is located in the SW CAOB and extends E-W from NW China to Kyrgyzstan, Tajikistan, and Uzbekistan for at least 2,500 km and is separated from the Junggar basin to the north and the Tarim basin to the south by two Cenozoic major fold-and-thrust belts (Figure 1b). It is generally considered to be formed in the Paleozoic through multiphase accretion of different microcontinents, island arcs, seamounts, and accretionary complex between the Kazakhstan and Tarim continents (Gao et al., 1998; Han et al., 2011; Shu et al., 2004; Wang et al., 2018).

The Chinese segment of the Tianshan belt is tectonically divided into three parts, namely, North Tianshan, Central Tianshan, and South Tianshan by two major ductile shear zones (Figure 1b). To the north, the North Tianshan Fault (NTF; Zhao et al., 2003) along the north boundary of the Yili Block extends eastward merging into the Main Tianshan Shear Zone (MTSZ; Laurent-Charvet et al., 2002, Laurent-Charvet et al., 2003) along the northern margin of the Central Tianshan. To the south, the Nalati Fault (NF)-Baluntai Fault-Xingxingxia Fault (Wang et al., 2014; Zhao et al., 2003) extend along the southern margins of the Yili and Central Tianshan blocks (Figure 1b). Displacements along these faults are considered as reactivations of the older suture zones during the Permian to Triassic and predominantly show dextral kinematics (de Jong et al., 2009; Laurent-Charvet et al., 2003; Wang et al., 2006; Wang et al., 2008; Wang et al., 2009; Yin & Nie, 1996).

The Turpan-Hami basin is bordered by the Bogda Belt and Barkol Tagh to the north and the Chol Tagh to the south (Figure 1b; Greene et al., 2005) and is mainly covered by Meso-Cenozoic sedimentary sequences (Figure 1c; XGSC, 2007). The upper Paleozoic strata are mainly exposed along its northern margin. Our sampling was carried out on Lower Permian strata from both Qijiaojing and Daheyan (DHY) areas that are located in the northern margin of the Turpan-Hami basin and are ~240 km apart from each other (Figure 1c). Paleomagnetic samples were oriented by both magnetic and solar compasses whenever possible. The average difference between these measurements is 1.6° ± 1.2°, which is applied to the cores without the solar measurement. Details of paleomagnetic sampling are presented in supporting information Table S1.

2.1. The Qijiaojing Area

Late Paleozoic and Mesozoic strata in the Qijiaojing area are composed of, from bottom to top, the Upper Carboniferous Julideneng Formation (C_{2j}), Shaleisaierke Formation (C_{2s}), and Yangbulake Formation (C_{2y}), the Lower Permian Kulai Formation (P_{1k}), and unconformably overlying Upper Jurassic Hongshan Formation (J_{3h}) (Figure 2a; XBGMR, 1973). The Kulai Formation is made up by dark gray purple olivine basalts with minor purple quartz porphyries in the upper part and purple-red siliceous conglomerates, reddish fine sandstones, acidic volcanic breccias, quartz porphyries, and andesitic porphyrites in the lower part (XBGMR, 1973).

The lower part of the Kulai Formation was sampled, and it consists of basalts, fine- and coarse-grained sandstones, and conglomerates containing rhyolitic clasts. In some geologic maps (XGSC, 2007), these rocks are assigned to be the Lower Permian Aerbasayi Formation (P_{1ae}). The strata are poorly exposed with a total thickness of about 1 km (Figure 2a). They generally strike ENE-WSW (253–264°) and dip to north with dip angles varying from 62° to 71°. Due to poor exposure, road conditions, and noncontinuous outcrop, a relatively small number of outcrops are accessible. Our samples were collected from two sections, which are stratigraphically ~200 m apart. From the southern section (Qijiaojing-A), 31 paleomagnetic cores from three sites (TH01 to TH03) and a cobble of rhyolite 15T123B were collected (Figures 2b and 4a); from the northern section (Qijiaojing-B), 32 paleomagnetic cores from four sites (TH11 to TH14) and a sandstone dating sample 15T124 were collected (Figures 2b and 4b). Individual sedimentary beds varying from 3 to 10 m with suitable lithology were selected as sampling sites, and 8 to 13 samples were taken from each site. In total, the strata covered by our sampling is thicker than 130 m (Figures 2b). Abundant sedimentary structures, such as load casts and rhythmic layering (Figures 4c and 4d), can be recognized on the outcrops and indicate overturned sequences.

2.2. The DHY Area

The Paleozoic strata from the DHY area include, from bottom to top, the Upper Carboniferous Liushugou Formation (C_{2l}), Qijiagou Formation (C_{2qj}), and Qiergusitao Formation (C_{2q}), the Lower Permian

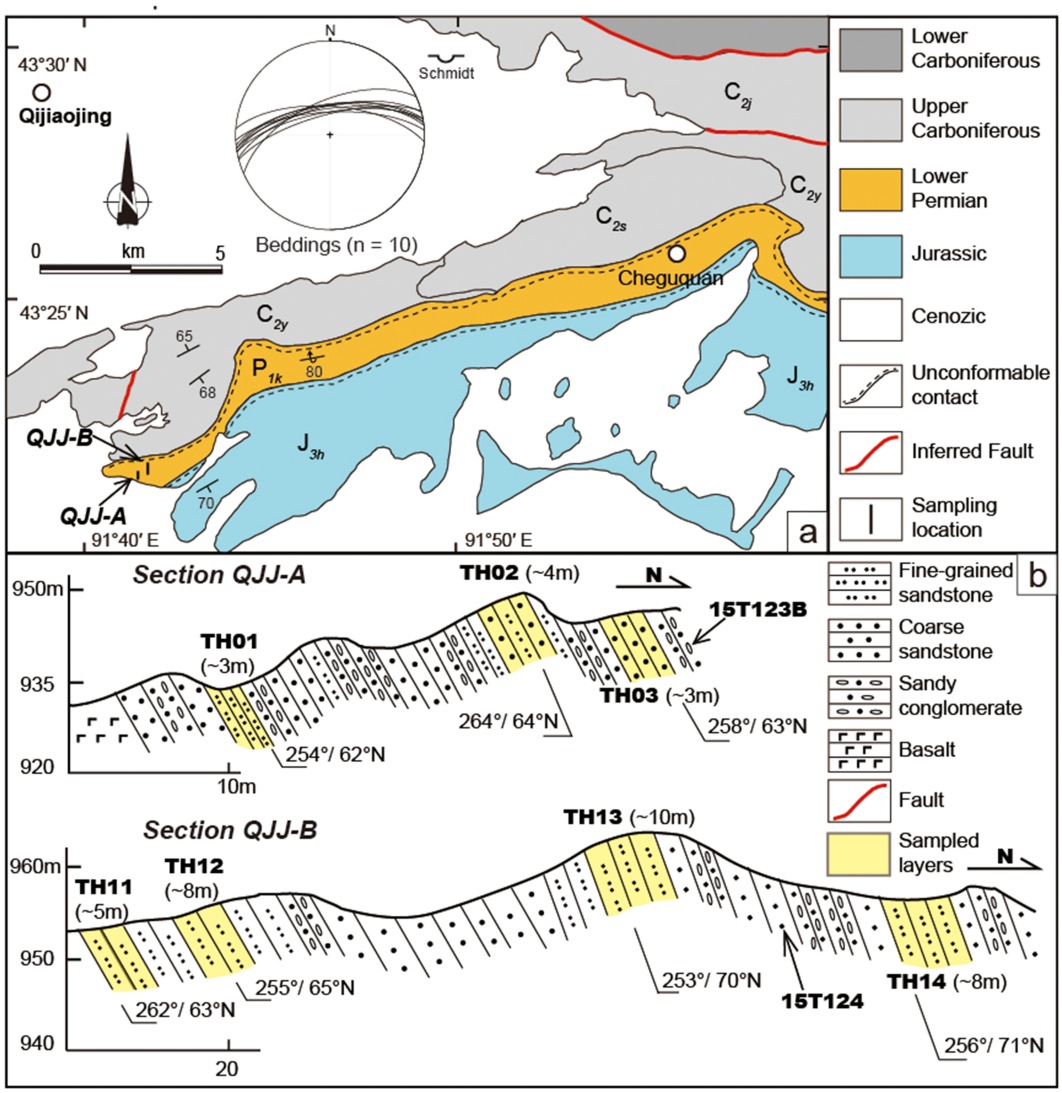

Figure 2. (a) Geologic map of the Qijiaojing area, north of the Turpan-Hami Basin (modified from XBGMR, 1973 and XGSC, 2007). QJJ-A and QJJ-B stand for two sampled sections. (b) Cross sections of two studied sections in the Qijiaojing area. stratigraphic positions of paleomagnetic sampling sites and geochronologic samples are shown. QJJ = Qijiaojing.

Aerbasayi Formation (P_{1ae}) and Tashikula Formation (P_{1t}), and the Lower-Middle Permian DHY Formation ($P_{1\text{-}2d}$) (XGSC, 2007). These strata are occasionally crosscut by late Paleozoic intrusive rocks (Figure 3a). The Aerbasayi Formation is unconformably underlain by or in fault contact with Carboniferous strata and only exposes in a limited area with a total thickness of around 1 km (Figure 3a); its lower part contains gray purple sandstones, sandy conglomerates, and tuffaceous conglomerates, interlayered with quartz porphyries, silicic volcanic breccias, and tuffs; its upper part is made up of gray purple andesites, andesitic, rhyolitic porphyries, and tuff sandstones (XGSC, 2007).

Two subsections were investigated and sampled, and their stratigraphic distance is ~500 m. The strata generally strike sub-E-W (258–297°) and dip subvertically (74–82°) either to the north or to the south (Figures 3b and 4e). As a result of poor exposure, road conditions, and noncontinuous outcrop, a relatively small number of sites were collected. In total, 24 paleomagnetic cores from three sites (TH18 to TH20) were collected from the southern section (DHY-A), which is composed of basalts and interbedded fine-grained sandstones (Figure 3b). Additional 25 paleomagnetic cores from three sites (TH15–TH17) were sampled from the northern section (DHY-B) that consists of gray sandstones and conglomerates (Figure 3b). Individual sedimentary beds varying from 3 to 10 m with suitable lithology and a 3 m andesitic basalt flow were chosen as sampling

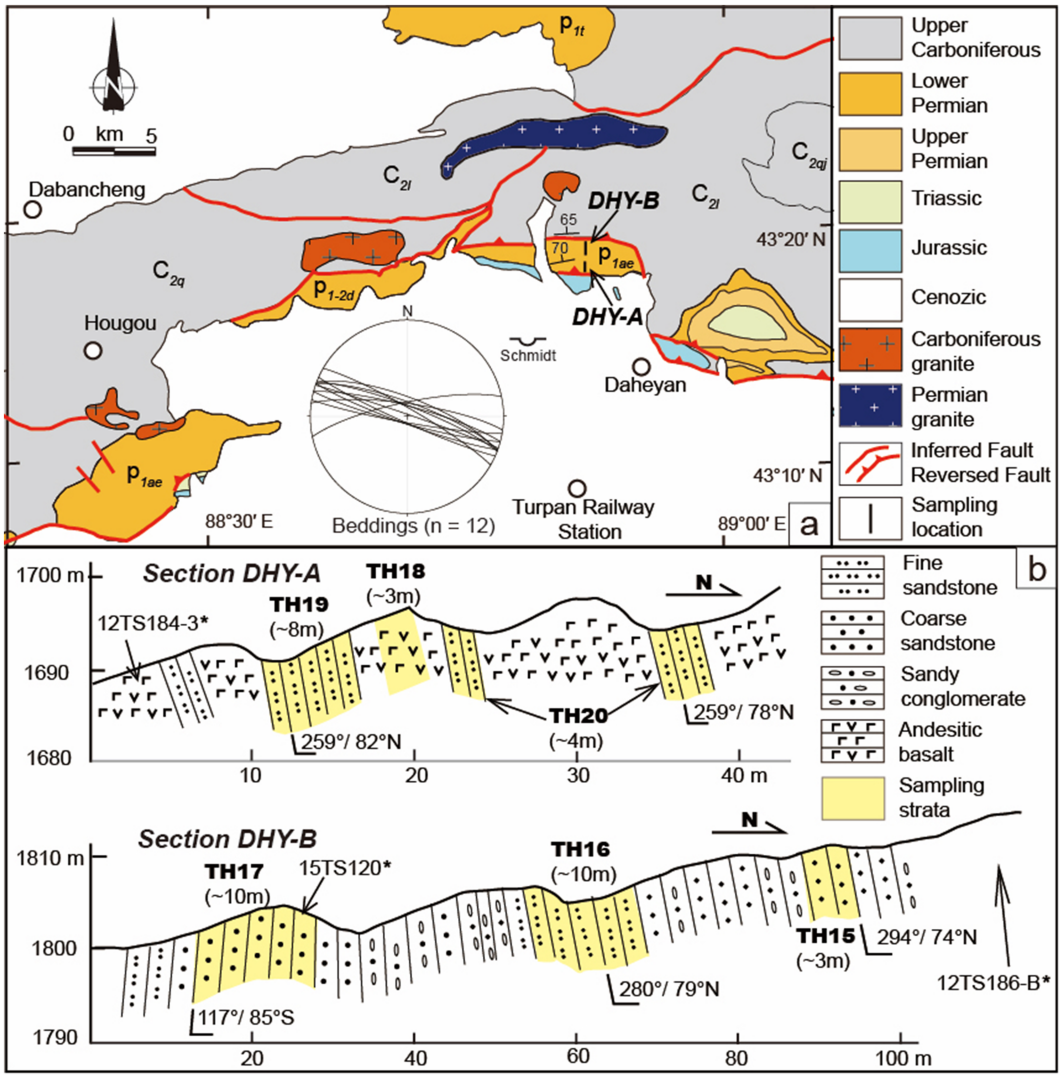

Figure 3. (a) Geologic map of the Daheyan area, NW of the Turpan-Hami Basin (modified from XBGMR, 1960, 1988 and XGSC, 2007). DHY-A and DHY-B stand for two sampled sections. (b) Cross sections of two studied sections in the Daheyan area. stratigraphic positions of paleomagnetic sampling sites and geochronological samples are shown. Note that geochronological samples labeled with * are after Wali et al. (2018). DHY = Daheyan.

sites, and 7 to 9 samples were obtained from each site. Our sampling covers around 110 m-thick strata (Figures 2b). Cross bedding (Figure 4f) and rhythmic layering can be observed in clastic rocks and along with the contact between the basalts and sandstones (Figures 4g and 4h). Overturned sequences are accordingly indicated for most strata except for site TH17. Subvertical sandy conglomerates and conglomerates (Figure 4i) occur between the studied sections.

Wali et al. (2018) provided a zircon U-Pb age for a rhyolite flow (297.9 ± 8.1 Ma) and a maximum deposition age of ~297 Ma for a sandstone, which were collected from strata lower than the DHY-B section and from Site H17, respectively (Figure 3b), indicating the oldest formation age at ~297 Ma for these strata. In addition, according to regional stratigraphic data (XBGMR, 1960, 1988; XGSC, 2007), our studied strata belong to the Aerbasayi Formation, and its formation age is reasonably constrained as Early Permian (297–273 Ma).

3. Rock Magnetism and Magnetic Fabric

In order to recognize the main remanence carriers of the studied samples, rock magnetic mineralogic analyses were conducted, including thermomagnetic experiments, hysteresis measurements, and isothermal

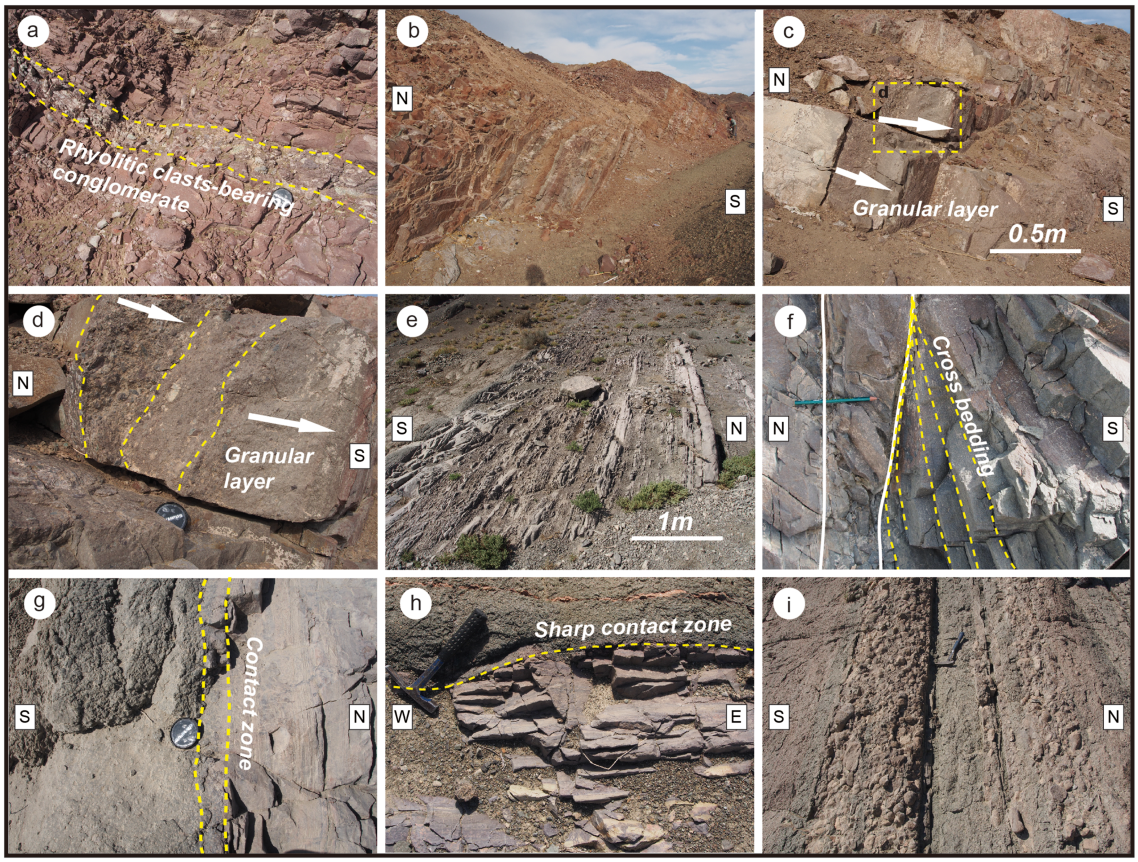

Figure 4. Field photographs of lower Permian strata in the Qijiaojing and Daheyan sections, northern margin of the Turpan-Hami Basin. (a,b) Sandstones and conglomerates including rhyolitic clasts in the Qijiaojing area; (c,d) rhythmic stratification indicating an overturned sequence; (e) subvertical beddings of volcanic and sedimentary rocks in the Daheyan area; (f) cross bedding in the sandstone; (g) contact between basalt and underlying baked and slightly hornfelsed sandstone and (h) overlying unbaked sandstone, suggesting an overturned sequence in the Daheyan area; and (i) subvertical beddings of sandy conglomerates and conglomerates exposed between sections DHY-A and DHY-B.

remanent magnetization (IRM) acquisition. In addition, magnetic fabric (anisotropy of magnetic susceptibility [AMS]) measurements were also carried out to test the reliability of the remanence and to allow possible detection and correction of inclination shallowing bias (Jackson et al., 1991). A detailed description of the methods is presented in Text S1.

3.1. Rock Magnetism

In light of the characteristics of magnetic mineralogic behaviors, our paleomagnetic samples are divided into three groups (A: TH01–TH03; B: TH11–TH14 & TH19–TH20; and C: TH15–TH18). For Group A, magnetic susceptibility increases with heating from room temperature to ~400 °C and then decreases with continuous heating up to 680 °C. Rapid decrease happens between 540 °C and 680 °C (Figure 5a). The hysteresis loops are wasp-waisted and not fully saturated at a maximum field of 500 mT (Figure 5b). These results indicate a mixture of low and high coercivity magnetic minerals (Roberts et al., 1995). The *Hc* (coercivity of all minerals) and *Hcr* (coercivity of remanence) values are both high, indicating a dominant high-coercivity component. IRM acquisition curves show a rapid increase of IRM below 50 mT, and IRM is not saturated at the maximum field of 1.5 T, indicating two magnetic phases contribute to the remanence (Figure 5c). Consequently, the magnetic remanence carrier for Group A is suggested to be hematite with minor magnetite.

Samples in Group B show high magnetic susceptibilities, and their thermomagnetic curves are similar to those of Group A (Figure 5d). A progressive increase of magnetic susceptibility during heating from room

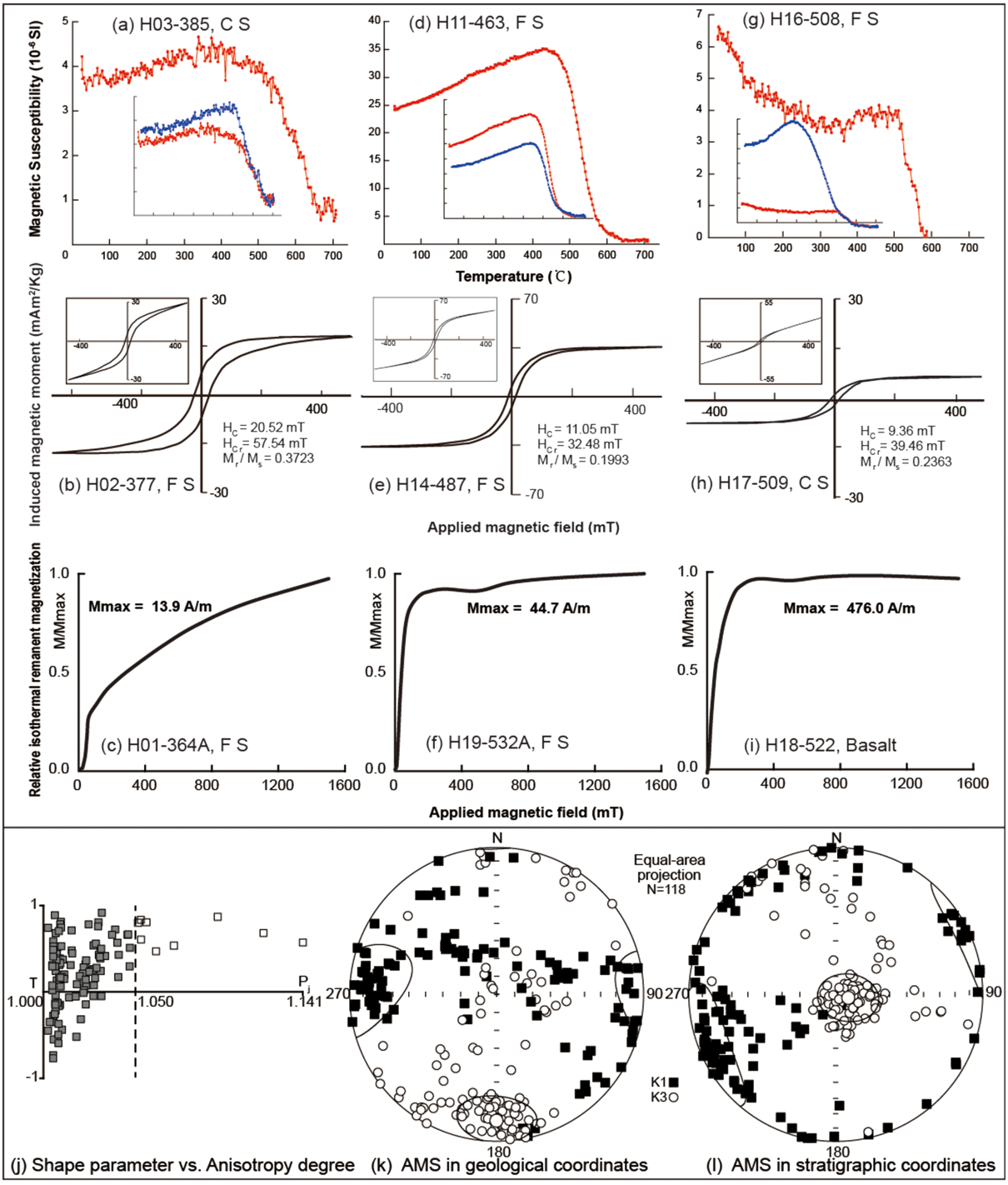

Figure 5. Representative rock magnetic analysis results and magnetic fabrics for the samples from the Qijiaojing and Daheyan sections, north of the Turpan-Hami Basin: (a, d, and g) results of thermomagnetic experiments. The red and blue curves were acquired during heating and cooling, respectively; (b, e, and h) magnetic hysteresis curves; (c, f, and i) acquisition curves of isothermal remanent magnetization; (j) plot of anisotropy degree (P_j) versus anisotropy shape (T) of magnetic susceptibility. Open squares represent nine specimens from site TH19; and (k and l) AMS orientations for 118 specimens in the geographic and stratigraphic coordinates. F S and C S stand for fine-grained sandstones and coarse-grained sandstones, respectively.

temperature to ~450 °C may be related to mineral transformations of sulfides (Roberts et al., 2011); rapid decrease with heating from 500 to 580 °C clearly shows the existence of magnetite (Dunlop et al., 1997); and further weak decrease when heated up to 640 °C may suggest the presence of minor hematite

(Figure 5d). The hysteresis loops are narrow, with the saturation below 400 mT (Figure 5e), corresponding to low H_c and H_{cr} values, revealing a dominant low-coercivity component. IRM acquisition curves reach 90% saturation at 200 mT, and IRM is not saturated until under a field of 1.5 T (Figure 5f). Therefore, magnetite and minor amount of hematite are the principal magnetic carriers for Group B.

Samples of Group C show a progressive decrease of magnetic susceptibility with heating from room temperature to 360 °C (Figure 5g), which agrees with the typical magnetic behavior of paramagnetic minerals (Curie Law; Tauxe et al., 2010); and subsequent increase with heating up to 520 °C could be due to mineral transformations of sulfides; the sharp decrease with continuous heating thereafter from 520 to 590 °C suggests the presence of magnetite (Figure 5g). The hysteresis loops are saturated below 200 mT; their low H_c and moderately high H_{cr} values imply that the magnetite grains are small (Figure 5h). IRM acquisition curves saturate at ~200 mT (Figure 5i), which consistently proves that magnetite is the major magnetic carrier for the samples of Group C.

3.2. Magnetic Fabric (AMS)

The magnetic fabrics were measured on a total of 118 specimens from both Qijiaojing and DHY areas. The magnetic susceptibilities of four basalt specimens vary from 2.64×10^{-2} to 5.02×10^{-2} SI, and those of other specimens range from 2.45×10^{-4} to 9.38×10^{-3} SI. The AMS results of all specimens show a magnetic fabric characterized by oblate ellipsoids (Figure 5j). Most specimens show P_J (anisotropy degree of AMS) values below 1.05, ranging from 1.002 to 1.047, with a mean of 1.012 (Figure 5j); and only nine specimens from Site TH19 reveal P_J values varying from 1.051 to 1.141 with a mean of 1.072.

Overall speaking, the in situ K_{max} axis (the maximum axes of the ellipsoid used to represent the magnetic anisotropy; magnetic lineation) shows a near E-W orientation (272.9° ± 31.9°; Figure 5k). After tilt correction, K_{min} axes (the minimum axes of the magnetic anisotropy ellipsoid; pole of magnetic foliation) cluster to be perpendicular to horizontal plane, and K_{max} axes scatter horizontally (Figure 5l), indicating that the oblate magnetic fabric is mainly related to the depositional process.

4. Paleomagnetism

At least seven specimens were selected from seven samples from each site for demagnetization. Both thermal and alternating field (AF) demagnetizations were carried out to isolate characteristic remanent magnetizations (ChRMs). Tilt corrections for overturned sequences were achieved by restoring the sequences to their original horizontal attitude (more specific, use opposite measured strike direction and supplementary angle of measured dip angle to conduct corrections in a paleomagnetic software). Related methods are described in Text S1 (Cogné, 2003; Deenen et al., 2011; Fisher, 1953; Kirschvink, 1980; Koymans et al., 2016; Zijderveld, 1967).

ChRMs are successfully isolated from ~85% of measured specimens; the remaining ~15% of the specimens show erratic demagnetization results due to weak magnetic remanence or thermal transition during heating; therefore, they were excluded from further analysis. Thermal and AF demagnetization diagrams of twin specimens from the same core are comparable (Figures 6a and 6b). Nevertheless, thermal demagnetization is generally more effective than AF one as the latter cannot completely isolate the remanence of hematite-bearing specimens (Figure 6a).

Depending on whether or not hematite is the main remanence carrier of specimens, the demagnetization results can be classified into two groups. For the specimens in which magnetite is the main remanence carrier, two components are easily isolated: The low-temperature or low-coercivity components are commonly removed at 200–250 °C or 10–20 mT; and the high temperature or high-coercivity components (ChRMs) are isolated from at least four successive steps in the interval of 400–590 °C or 20–100 mT (Figures 6c and 6d).

For the specimens with hematite as a main remanence carrier, the low-temperature or low-coercivity components are also unblocked at 200–250 °C or 10–20 mT. However, their ChRMs are complicated and three cases are recognized. (1) Most specimens show ChRMs isolated from at least five steps in the interval 400–690 °C or 20–150 mT (Figures 6e and 6f). (2) A few specimens reveal a slight direction difference between the components isolated in the 400–590 and 590–690 °C intervals (Figure 6g). Their demagnetization curves from 400 to 590 °C are straight, indicative of a single component; and those from 590 to 690 °C

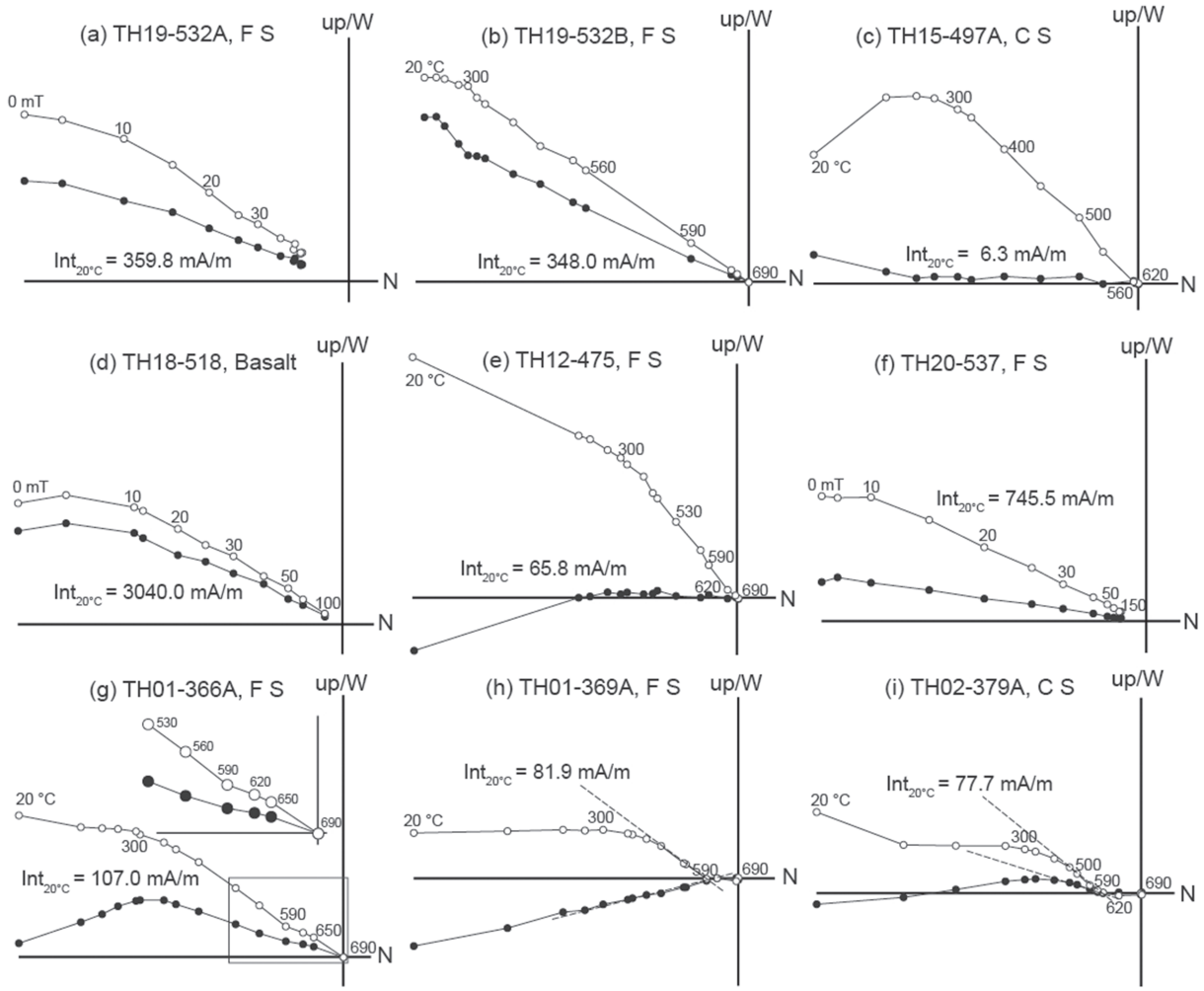

Figure 6. Representative demagnetization diagrams for sedimentary and volcanic rocks collected from the Qijiaojing and Daheyan sections, north of the Turpan-Hami Basin. All demagnetization plots are displayed after bedding tilt corrections. Solid (open) symbols stand for the projection of vector end points on the horizontal (vertical) plane. F S and C S stand for fine-grained sandstones and coarse-grained sandstones, respectively.

are curvilinear, likely due to a superposition effect of two components, similar to descriptions in Butler (1992). Because their remanence directions are almost the same, the ChRMs were analyzed by using 450–690 °C interval with forcing the fitting line toward the origin. (3) The remaining specimens demonstrate two significantly different high-temperature components isolated in 400–590 and 590–690 °C intervals (Figures 6h and 6i). The remanence directions of the 400–590 °C component are consistent with other ChRMs and can be considered as the ChRMs of these samples. Whereas the 590–690 °C components generally show a shallow inclination and a declination of ~180°, which are completely different from the ChRMs acquired from other specimens, thus, they are regarded as a possible secondary remanence, and their importance will be discussed later.

All the isolated ChRMs yield a reverse polarity. Estimated site-mean directions are listed in Table S1. In the Qijiaojing area, the ChRMs of the two sections are consistent, resulting in a tilt-corrected mean remanence direction of $D \pm \Delta D = 179.6° \pm 3.9°$, $I \pm \Delta I = -39.7° \pm 5.0°$ ($n = 63$, $k = 26.0$, $\alpha_{95} = 3.6°$) (Figure 7a and Table S1). Two sections in the DHY area show significantly different mean remanence directions (Figure 7c). The mean direction of the section DHY-A is calculated as $D \pm \Delta D = 205.3° \pm 2.7°$, $I \pm \Delta I = -33.0° \pm 4.1°$ ($n = 25$, $k = 113.3$, $\alpha_{95} = 2.7°$; Figure 7c and Table S1), whereas the one obtained at the Section DHY-B is $D \pm \Delta D = 178.3° \pm 4.4°$, $I \pm \Delta I = -50.6° \pm 4.2°$ ($n = 35$, $k = 48.4$, $\alpha_{95} = 3.5°$; Figure 7c and Table S1). The isolated low-temperature or low-coercivity components are more concentrated in geographic coordinates (mean

direction: $D = 6.5°$, $I = 63.5°$, $\alpha_{95} = 1.8°$, $n = 80$), which is indistinguishable with the present Earth field ($D = 2.0°$, $I = 63.8°$; PaleoMac; Thébault et al., 2015), than in stratigraphic coordinates (mean direction: $D = 172.2°$, $I = 6.3°$, $\alpha_{95} = 5.3°$, $n = 80$) (Figure S1).

5. Zircon U-Pb Geochronology

Two samples for zircon U-Pb dating were prepared and analyzed at the LA-ICP-MS Laboratory of the State Key Laboratory for Mineral Deposits Research (SKLMDR, Nanjing University). Related methods are described in Text S1 (Black & Gulson, 1978; Andersen, 2002; Jackson et al., 2004; Ludwig, 2001). The cathodoluminescence (CL) images of dated zircons and analytical results are reported in Figures S2 and S3 and Table S2.

For the Rhyolitic Cobble Sample 15T123B collected from the Kulai Formation, the dated zircons are 80–200 μm in size and have subhedral to euhedral shapes with length/width ratios of 1.5–3, and their CL images generally show clear oscillatory zonings, which indicate an origin from a siliceous melt (Figure 8a and Figure S2). Seventeen concordant zircons yielded 16 consistent apparent ages, and a weighted mean age is calculated at 310.5 ± 1.2 Ma with MSWD = 0.61 (Figures 8a and 8b). One exceptional older age (327 ± 5 Ma) was obtained from Zircon No. 12 (Figure 8a and Table S2), whose CL image is plain dark without oscillatory zoning, and this zircon should have derived from different source. Therefore, the depositional age of this formation should be younger than about 310 Ma.

Detrital zircons from the Sandstone Sample 15T124 are 50–200 μm in size and have subrounded to subeuhedral shapes with length/width ratios of 1–3 (Figure S3). Their CL images are generally black or bright with concentric oscillatory zonings; however, some zircons have plain dark CL images, and no oscillatory zoning is visible (Figure S3). Fifty concordant ages ranging from ~293 Ma (Nos. 4, 7, 35, and 46; Figure 8c) to 1,145 Ma (No. 50) are acquired, which define a uniform peak at ~308 Ma (Figures 8c and 8d and Table S2). The weighted mean age of the youngest four zircons is calculated at 293.9 ± 2.0 Ma (Figure 8d). Thus, the maximum depositional age of the sandstone could be approximated as 294 Ma.

6. Discussion

6.1. Inclination Shallowing Test

Inclination shallowing can occur in sedimentary rocks due to compaction and/or rock-magnetic effects and has been frequently documented in previous studies (e.g., Kodama, 2012). A test of possible inclination shallowing is therefore indispensable for paleomagnetic studies on sedimentary rocks in order to obtain reliable tectonic implications (e.g., Huang et al., 2015). Two most widely used correction methods are the elongation/inclination (E/I) correction of the ChRM distribution (Tauxe et al., 2008; Tauxe & Kent, 2004) and the one based on AMS or remanence (Jackson et al., 1991; Kodama, 2009).

The E/I correction is based on the paleosecular variation (PSV) models TK03 (Tauxe & Kent, 2004). Since the DHY and Qijiaojing areas are ~240 km apart, their E/I corrections were separately conducted. For the strata in the Qijiaojing area, according to the Deenen et al. (2011) criteria, the distribution of the ChRM directions reflects the contribution from PSV of the geomagnetic field (i.e., $A_{95\ \mathrm{min}} = 2.3° < A_{95} = 3.6° < A_{95\ \mathrm{max}} = 6.0°$; Figure 7b). This indicates that tectonic-induced scattering or remagnetization can be ruled out. The plot of elongation versus inclination for these data (dashed) and for the TK03.GAD model (solid) is shown in Figure 9a. The crossing points represent the inclination/elongation pair most consistent with the TK03.GAD. Consequently, the flattening factor f ($\tan I_c = f \tan I_o$, where I_c and I_o are the compacted and original inclinations; Jackson et al., 1991) is obtained as 0.75, and the mean inclination is corrected from −39.7° ± 5.0° to −47.3° with 95% confidence limits between −40.0° and −56.1° (Figures 9b and 9c).

Mean ChRMs from two sections are significantly different in the DHY area (Figure 7c). For the Section DHY-A, the PSV is underrepresented within site and among sites ($A_{95} = 2.6° < A_{95\ \mathrm{min}} = 3.3°$; Figure 7e and Table S1). Specimens from Site TH18 were collected from a ~3 m-thick basalt flow (Figure 3b), and their site-mean direction can be therefore regarded as a spot record of paleo-geomagnetic field. Considering that basalt flows and sandstones are interbedded in the Section DHY-A (Figure 3b), remagnetization of the Sandstone Sites TH19 and TH20 caused by the overlying basalts could have resulted in their underrepresentation of the PSV. This assumption is also supported by the straightforward demagnetization curves of the

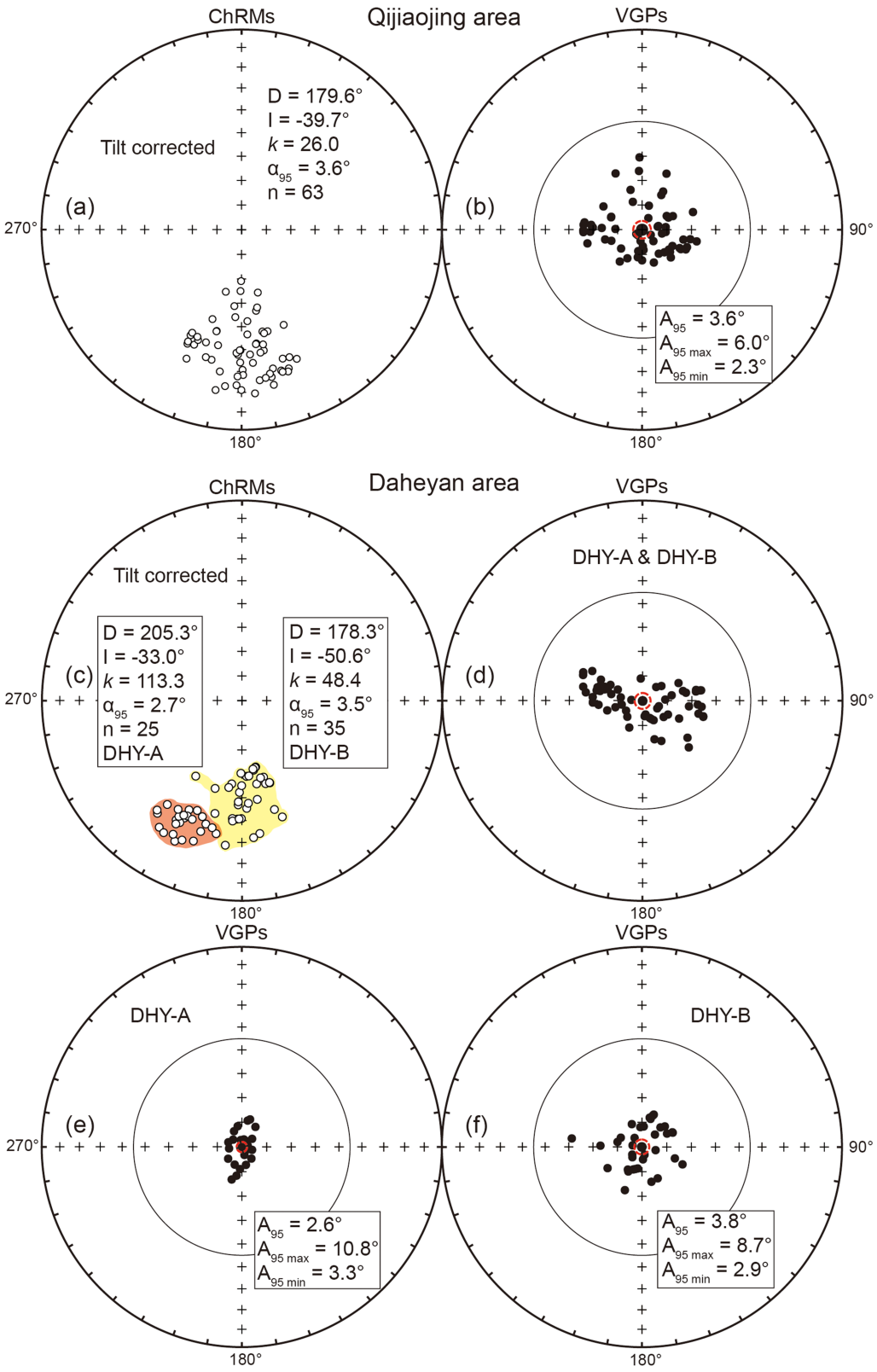

Figure 7. Equal-area projections of the isolated ChRM directions in stratigraphic coordinates from the Qijiaojing section (a) and Daheyan (DHY-A and DHY-B) section (c) and the corresponding VGPs for the Qijiaojing section (b), Daheyan (DHY-A & DHY-B) section (d), DHY-A section (e), and DHY-B section (f). Cutoff criterion of 45° is used after Deenen et al. (2011).

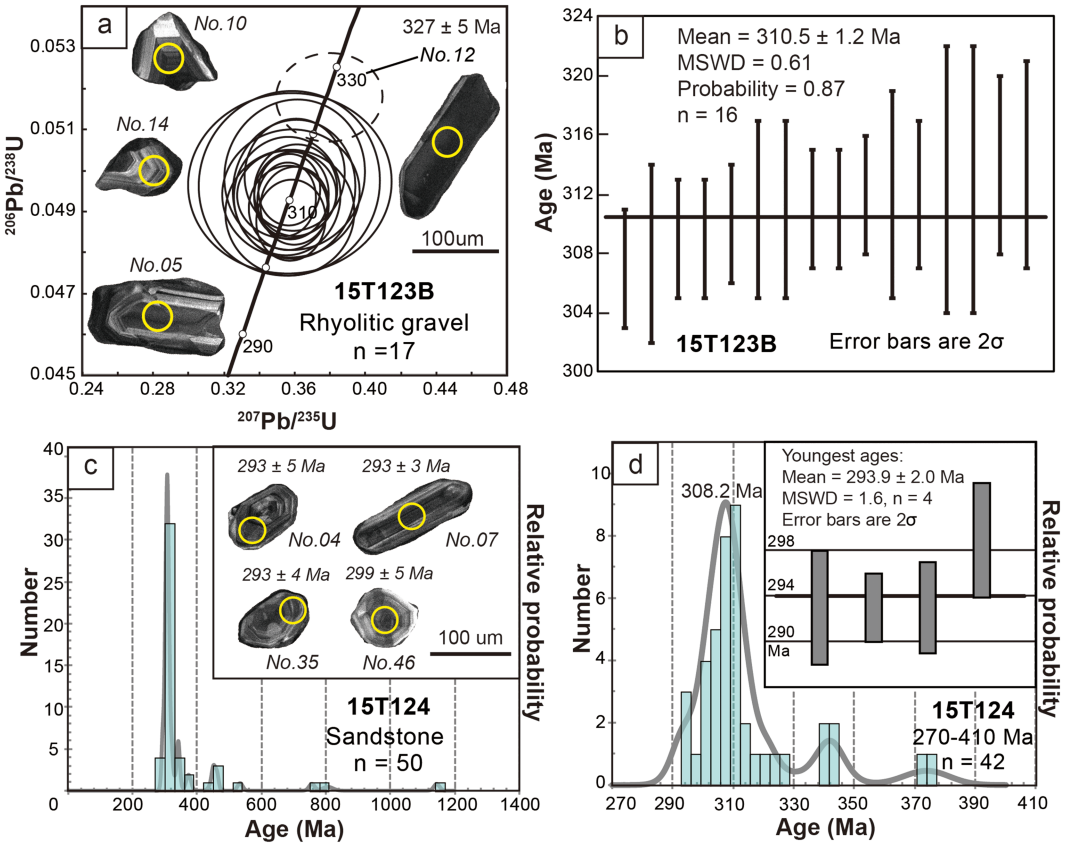

Figure 8. (a) Concordia diagram of zircon U-Pb dating and cathodoluminescene images of representative zircons for the rhyolitic cobble sample 15T123B from the conglomerate of the Qijiaojing area; (b) weighted mean zircon U-Pb age for sample 15T123B calculated from 16 out of 17 individual ages; (c) histogram and relative probability curve for detrital zircon U-Pb ages of the sandstone sample 15T124 from the Qijiaojing area, the cathodoluminescence images of the youngest zircons are shown; (d) probability density function plot of sample 15T124 shown in 270–410 Ma window and the weighted mean age calculated from the youngest ages.

corresponding specimens (Figures 6a, 6b, and 6f). Hereby, their site-mean directions should be also regarded as spot records of the paleo-geomagnetic field. Consequently, we combined the site-mean directions of Sedimentary Sites TH19 and TH20 with 35 single directions from the Section DHY-B, where the PSV is fully represented ($A_{95\ \mathrm{min}} = 2.9° < A_{95} = 3.8° < A_{95\ \mathrm{max}} = 8.7°$; Figure 7f), to perform an E/I correction. The result shows no intersection between the elongation-inclination curve of our data and that of the geomagnetic TK03 field model (Figure 9d). Combining with its subcircularly distributed VGPs, the strata in the DHY area did not experience inclination shallowing (Figures 9e and 9f).

Although Tauxe et al. (2008) suggested that data sets smaller than ~100–150 independent samples give less reliable result for an E/I correction and that the validity of TK03 model in the Paleozoic is still unclear, as there is no relevant work conducted on the studied strata, our correction provides up to now the first and preliminary constraint on the inclination shallowing effect of the Permian strata in the Turpan-Hami Basin. In addition, our tentative E/I correction on Cretaceous poles of Turpan-Hami and South Junggar blocks indicates that even for a data set of ~20, meaningful results can be acquired when only the mean value is considered (Text S2, Figure S5, and Table S3).

The AMS or remanence can also be used to correct inclination shallowing, and its accuracy relies on measuring the anisotropy of only ferrimagnetic minerals that carry the ChRMs. In our case, the mean magnetic susceptibility of the specimens is 1.1×10^{-3} [SI], suggesting that the AMS is controlled by both ferrimagnetic and paramagnetic minerals (Tarling & Hrouda, 1993). Therefore, any correction based on AMS is unsuitable for this study.

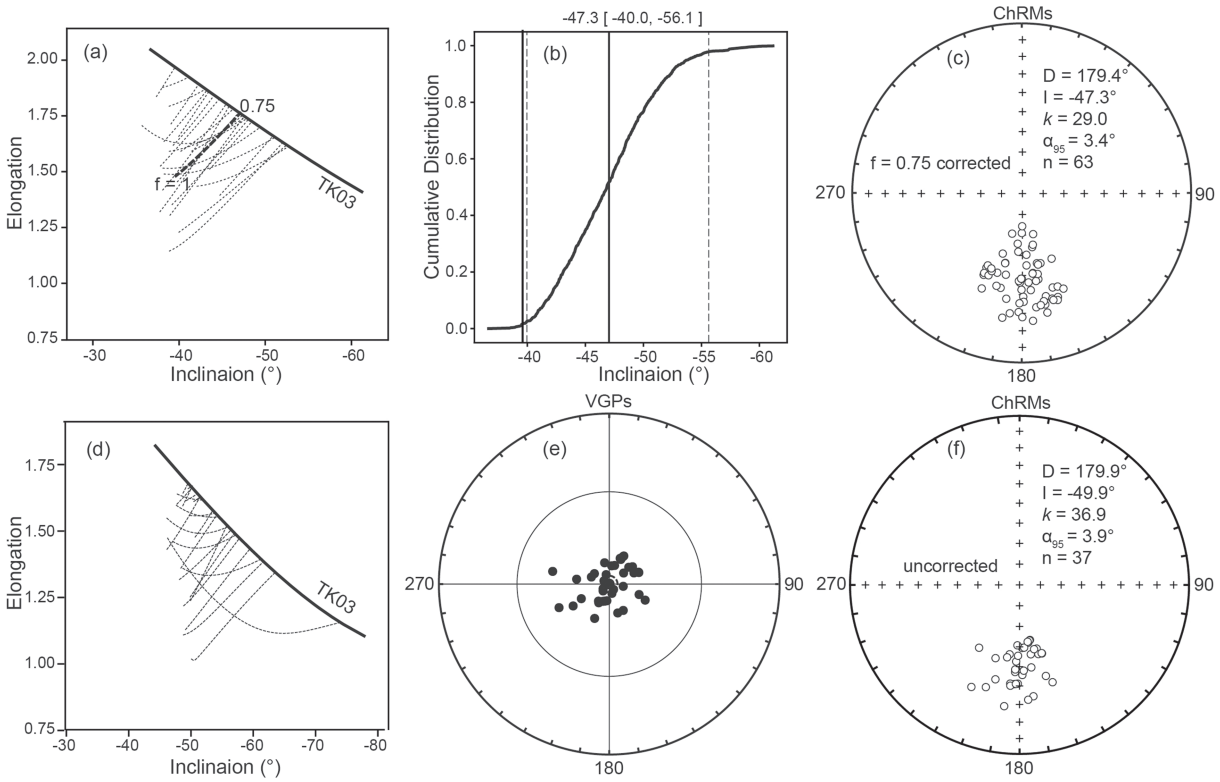

Figure 9. E/I corrections on the paleomagnetic specimens from the Qijiaojing area (a–c) and Daheyan area (d–f). (a) Plot of elongation versus inclination for the TK03.GAD model (solid line) and the data from the Qijiaojing area (dashed line). Twenty bootstrapped data sets are also shown. The crossing points represent the inclination/elongation pair most consistent with the TK03.GAD model. (b) Cumulative distribution of crossing points from 1,000 bootstrapped data sets. The dashed lines indicate the 95% confidence interval. (c) Equal-area projections of corrected ChRM directions in stratigraphic coordinates. (d) No intersection was found between the TK03.GAD model and the data from the Daheyan area. (e, f) Equal-area projections of VGPs and ChRMs, respectively, for the data from the Daheyan area in stratigraphic coordinates.

6.2. Magnetic Remanence Age and Paleomagnetic Pole Calculation

Due to the limited variation in bedding attitude in the studied strata (Table S1), inconclusive fold tests sensu stricto were acquired using site-mean directions (McElhinny, 1964). Therefore, a generalized nonparametric fold test was carried out on single ChRMs (Tauxe & Watson, 1994), and this yielded a positive result with the maximum clustering reached at 94–109% unfolding (Figure S4), suggesting a pretilt origin of the remanence. However, the fold test can only constrain a pretilt remanence, and the remanence age is still undeterminable as the age of tilting is difficult to date. Thus, further considerations are required to provide better constraints for the remanence age.

Demagnetization results of the hematite-bearing specimens show three kinds of behaviors (Figure 6), which most likely resulted from different formation mechanisms of hematite in sedimentary rocks (Butler, 1992; Kodama, 2012). (1) In some red sandstones, specular hematite likely exists as a primary mineral and carries a detrital remanence which was also recorded by detrital magnetite (Figures 6e and 6f). (2) Pigmentary hematite with submicron size is secondary and shows characteristic color of red beds. In the case that the pigmentary hematite formed within 10^3–10^4 years of deposition, its chemical remanence magnetization can still be a useful paleomagnetic signal (Kodama, 2012); but the chemical remanence magnetization may be slightly different from the ChRM carried by primary detrital hematite. Thus, the slightly curved demagnetization plots between 590 and 690 °C could be the result of superposition of remanences from different phases of hematite (Figure 6g). (3) Pigmentary hematite formed much later (e.g., postdepositional weathering/oxidation under low temperature condition) may carry a remanence that substantially differs from a primary one. In addition, because hematite has a high blocking temperature, its remanence may act as noise to hamper the accurate ChRM isolation (Figures 6h and 6i).

These demagnetization behaviors indicate that the isolated ChRMs we report should be primary ones. Moreover, the ChRMs may be acquired during or slightly later (10^3–10^4 years) than the time of deposition. Several lines of evidence, including low AMS, fully representation of the PSV by ChRMs (except the Section DHY-A), significant inclination shallowing of the strata in the Qijiaojing area, and sole reverse polarity of ChRMs (consistent with the Kiaman Reversed Superchron; Belica et al., 2017), all support a primary origin, that is, the remanence age should be approximately the same as the formation age of the studied strata.

In the Qijiaojing area, the Rhyolitic Cobble Sample 15T123B (310.5 ± 2.4 Ma) and Sandstone Sample 15T124 (maximum depositional age: 293.9 ± 2.0 Ma) provide an oldest formation age for the Kulai Formation at ~294 Ma (Figure 8). Together with regional stratigraphic data (XBGMR, 1960; XGSC, 2007), the formation age of the strata can be reasonably constrained as between 294 and 273 Ma. Combined with the Early Permian deposition age of the studied strata in the DHY area (297–273 Ma; Wali et al., 2018), the magnetic remanence age of our specimens is determined to be Early Permian.

To estimate a high-quality and reliable paleomagnetic pole, three factors were taken into consideration. First, the inclination-corrected ChRMs of specimens from the Qijiaojing area were used in the calculation in order to minimize effects of inclination shallowing. Second, as discussed above, the ChRMs of the specimens from the Section DHY-A only provide spot records of the paleo-geomagnetic field and is incomplete instead of the centered axial dipole; therefore, their mean direction significantly deviates from those obtained from other sites of coeval strata in the DHY and Qijiaojing sections (Figures 7a, 7c, and 10b). In addition, the distribution of ChRMs from the DHY area (Figure 7c) possibly suggests syndepositional local tectonic movements as indicated by the thick conglomerate layers between the two sections (Figure 4i). Thus, the results from the DHY-A section are excluded from the pole calculation. Third, because the site-mean VGPs are more circularly distributed than the site-mean directions (Deenen et al., 2011; Tauxe & Kent, 2004), paleomagnetic poles were calculated using Fisher (1953) statistics on the site-mean VGPs (Figures 10c and 10d and Table 1), which were derived from the site-mean directions (Figures 10a and 10b and Table 1). Consequently, the first Early Permian paleomagnetic pole for the Turpan-Hami Block was obtained as 75.7°N, 276.3°E, $A_{95} = 5.7°$, $K = 72.8$, and $N = 10$ sites (Figure 10d and Table 1).

6.3. Kinematic Constraints on the Intracontinental Tectonics of the SW CAOB

With the goal of a better understanding of the kinematic evolution among major blocks (the Yili, South Junggar, Tarim, and Turpan-Hami blocks) in Central Asia, we compiled published paleomagnetic poles and recalculated the mean poles for these blocks (Table S4; see details in Text S2; Bai et al., 1987; Li et al., 1988, Li et al., 1991; Sharps et al., 1989, Sharps et al., 1992; Chen et al., 1991, Chen et al., 1992; Nie et al., 1993; Cogné et al., 1995; Li et al., 1995; Fang et al., 1996, Fang et al., 1997, Fang et al., 2001; Meng et al., 1998; Gilder et al., 2003; Tan & Kodama, 2003; Huang, Wang, & Zhu, 2004; Tauxe & Kent, 2004; Choulet et al., 2011, Choulet et al., 2013; Zhao et al., 2014; Zhu et al., 2018). The Early Permian pole of the Turpan-Hami Block that we report is significantly different from those of South Junggar and Tarim, with angular differences of 22.0° ± 7.2° and 35.0° ± 5.9°, respectively. However, the Early Permian poles of the Turpan-Hami and Yili blocks are undistinguishable with an angular difference of 6.6° ± 9.0° (Figure 11a and Table 2). Cogné et al. (1995) and Huang, Wang, and Zhu (2004) have published Cretaceous paleomagnetic results for the Turpan-Hami Block. Taking into account the possible inclination shallowing of their data (Text S2, Figure S5, and Tables S3 and S4), the Cretaceous paleomagnetic pole of the Turpan-Hami Block is nearly undistinguishable from results from the Junggar and Tarim blocks with angular differences of 1.7° ± 5.1° and 5.7° ± 5.1°, respectively (Figure 11b and Table 2).

Our study provides the first Early Permian paleomagnetic pole for the Turpan-Hami Block, allowing us to discuss late Paleozoic paleogeographic position of this block and its movement with respect to surrounding crustal elements. The insignificant angular difference of 6.6° ± 9.0° between the Early Permian paleomagnetic poles of Turpan-Hami and Yili blocks corresponds to relative latitudinal movement of 6.1° ± 9.0° and relative rotation of −4.2° ± 10.9° (Table 2), which are unrecognizable within errors, suggesting that these two blocks have likely maintained approximate relative positions since the Early Permian.

Nevertheless, the observed large angular difference of 35.0° ± 5.9° between the Early Permian paleomagnetic poles of Turpan-Hami and Tarim (Table 2) indicates significant relative movements between these blocks since the Early Permian. Such significant relative movement is essentially represented by a

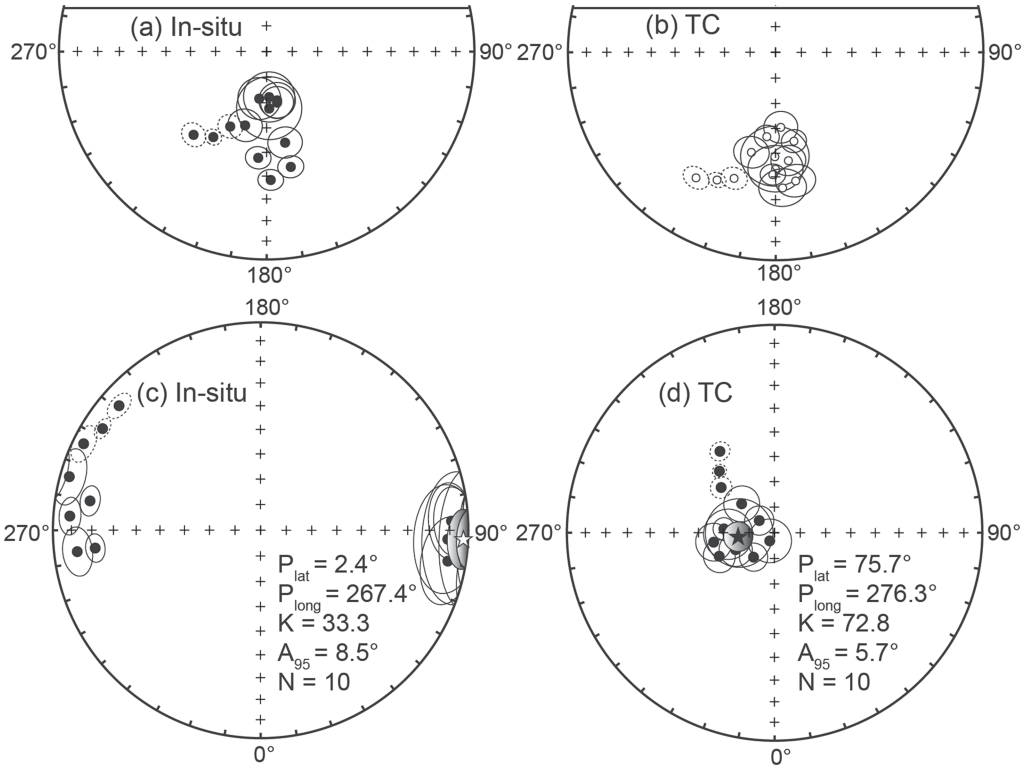

Figure 10. Equal-area projections of site-mean magnetic remanent directions in (a) geographic and (b) stratigraphic coordinates and corresponding visual geomagnetic poles in (c) geographic and (d) stratigraphic coordinates of the Early Permian paleomagnetic samples from the Qijiaojing and Daheyan areas, northern margin of the Turpan-Hami Basin. Noting that the dashed circles stand for sites H18–H20 which were sampled from the QJJ-A section.

Table 1
Paleomagnetic Results of Early Permian Samples From Turpan-Hami Basin (Inclination Shallowing Corrected)

Section	Site	n/n$_0$ (N)	D$_g$ (°)	I$_g$ (°)	D$_s$ (°)	I$_s$ (°)	k	α_{95} (°)	Plat$_g$ (N°)	Plong$_g$ (E°)	A_{95g} (°)	Plat$_s$ (N°)	Plong$_s$ (E°)	A_{95s} (°)
Qijiaojing area														
QJJ-A	TH01	13/14	202.5	58.5	193.4	−49.1	41.5	6.5	4.9	254.4	8.3	72.9	228.8	7.0
	TH02	9/10	188.1	72.0	179.9	−43.3	28.2	9.9	10.6	87.2	16.4	71.8	272.0	9.7
	TH03	8/8	178.4	70.1	173.1	−46.5	78.1	6.3	7.5	92.6	10.1	73.4	293.6	6.5
QJJ-B	TH11	6/12	186.5	67.6	180.3	−48.5	29.8	12.5	4.1	87.6	19.1	76.1	270.6	13.3
	TH12	12/12	174.1	53.8	175.8	−60.4	47.1	6.4	12.1	276.7	7.5	86.3	329.7	8.5
	TH13	7/11	199.2	70.5	176.9	−35.1	54.6	8.2	9.4	80.6	13.2	65.8	278.9	7.2
	TH14	8/13	178.2	70.9	171.0	−37.6	63.4	7.0	8.7	92.7	11.4	66.4	293.1	6.3
Daheyan area														
DHY-B	TH15	11/11	189.3	47.2	185.8	−56.5	97.4	4.6	17.8	260.3	4.8	82.4	231.6	5.7
	TH16	12/12	172.5	43.5	168.2	−54.1	87.5	4.7	21.0	276.2	4.6	77.4	319.4	5.5
	TH17	12/12	183.9	57.3	181.2	−40.9	94.3	4.5	8.7	265.8	5.6	70.1	265.7	4.3
DHY-A	TH18	7/7	224.6	43.3	212.3	−29.5	169.7	4.6	10.2	228.7	4.5	51.1	213.9	3.8
	TH19	12/14	216.1	47.9	204.5	−33.1	189.7	3.2	10.5	237.3	3.4	57.4	221.9	2.7
	TH20	6/8	211.2	55.4	198.1	−36.5	204.8	4.7	5.8	244.0	5.7	62.5	229.8	4.2
Mean^3		3/13	217.8	49.0			115.1	11.5	8.9	236.7	12.3			
					205.2	−33.2	137.6	10.6				57.2	221.1	10.9
Mean^{13}		13/13	194.2	59.5			31.9	7.5	4.0	260.4	9.7			
					185.6	−44.7	34.3	7.2				73.3	254.7	7.6
Mean^{10}		10/13	184.5	61.5			48.5	7.0	2.4	267.4	8.5			
					178.4	−47.4	72.1	5.7				75.7	276.3	5.7

Note. n/n$_0$ (N), number of specimens (sites) in calculation/totally studied. D$_g$, I$_g$, D$_s$, and I$_s$, declination (D) and inclination (I) in geological ($_g$) and stratigraphic ($_s$) coordinates; k, precision parameter; α_{95}, 95% confidence interval. Plat$_g$, Plong$_g$, Plat$_s$, Plong$_s$ and A_{95}, latitude and longitude of paleomagnetic poles in geographic ($_g$) and stratigraphic ($_s$) coordinates and 95% confidence interval. Mean^3, the mean calculation of the sites from the DHY-A section (Sites TH18–20). Mean^{13} and Mean^{10}, the mean calculation with and without Mean^3. Mean^{13} is statistically equal to Mean^{10} at 95% confidence level, with an angular difference of 5.1° ± 7.0°. However, in order to be more accurate, we apply Mean^{10} in further study.

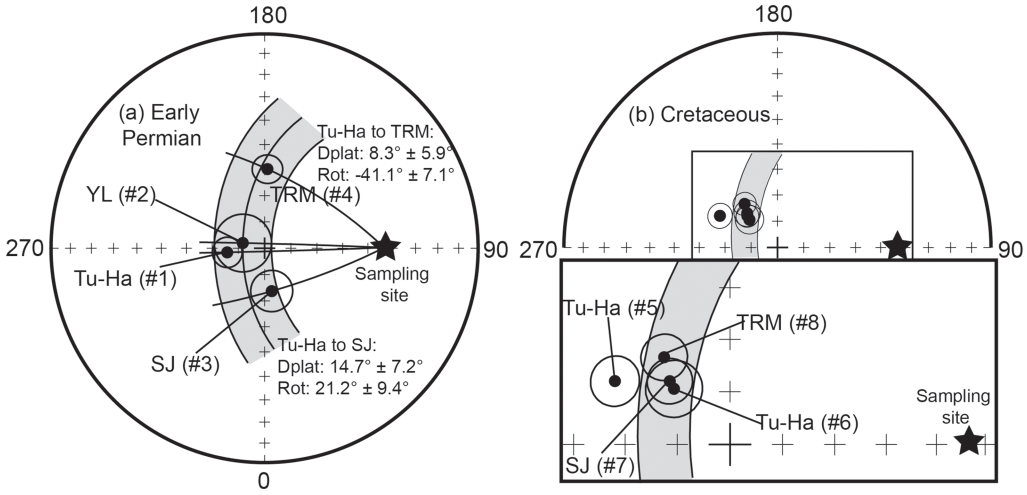

Figure 11. Equal-area projections of paleomagnetic poles of the Turpan-Hami (Tu-Ha), Yili (YL), South Junggar (SJ), and Tarim (TRM) blocks in (a) the Early Permian and (b) Cretaceous. Reference numbers (#no.) stand for different paleomagnetic poles listed in Tables 2 and S4, which are consistent. Relative movements between different paleomagnetic poles are shown in Table 2.

counterclockwise rotation of 41.1° ± 7.1° of the Turpan-Hami Block with respect to Tarim and by a relatively small latitudinal movement of 8.3° ± 5.9° (Table 2). Similar large counterclockwise rotations were also documented for the Yili Block with respect to Tarim from the Late Carboniferous to the Late Permian and were interpreted as the result of the large-scale dextral strike-slip movements between the Yili and Tarim blocks (Wang et al., 2007; Zhu et al., 2018). In fact, large-scale strike-slip shearing and related transpression and/or transtension were documented to be the principal pattern of the intracontinental tectonics in the SW CAOB (Allen et al., 1993; Choulet et al., 2011; Choulet et al., 2013; Laurent-Charvet et al., 2002; Laurent-Charvet et al., 2003; Wang et al., 2007, 2009; Wang et al., 2014; Zhu et al., 2018). Considering that the Turpan-Hami and Yili blocks may have kept their relative position since the Early Permian, these two blocks could have subsequently experienced a similar kinematic evolution. Therefore, this counterclockwise relative rotation of about 40° between the Turpan-Hami Block and Tarim can also be accommodated by large-scale right-lateral strike-slip movements along the NF-MTSZ. This hypothesis is supported by (1) structural and kinematic studies which show that ductile shearing along the MTSZ has been of dextral sense (Laurent-Charvet et al., 2002; Laurent-Charvet et al., 2003; Wang et al., 2007, 2014; Yin & Nie, 1996) and (2) multimineral $^{40}Ar/^{39}Ar$ dating on mylonitic rocks from the MTSZ yields cooling ages ranging from 290 to 245 Ma (de Jong et al., 2009; Laurent-Charvet et al., 2003). As for the relatively small latitudinal difference of 8.3° ± 5.9° between the Turpan-Hami and Tarim blocks, it can be considered as the result of a northward relative movement of the Turpan-Hami Block together with the Yili Block with respect to the Tarim Block that might have occurred as a simple "sliding" along the NE-SW-striking NF-MTSZ, instead of crustal shortening (Zhu et al., 2018).

Table 2
Relative Movements of the Turpan-Hami Block With Respect to the Surrounding Blocks

Period	Blocks	Angular difference (°)	Plat ± Δplat (°)	Rot ± Δrot (°)
Early Permian (present)	TH (#1) vs. YL (#2)	6.6 ± 9.0	6.1 ± 9.0	−4.2 ± 10.9
	TH (#1) vs. SJ (#3)	22.0 ± 7.2	14.7 ± 7.2	21.2 ± 9.4
	TH (#1) vs. TRM (#4)	35.0 ± 5.9	8.3 ± 5.9	−41.1 ± 7.1
Cretaceous (present)	TH (#6) vs. SJ (#7)	1.7 ± 5.1	−1.0 ± 5.1	−1.6 ± 6.0
	TH (#6) vs. TRM (#8)	5.7 ± 5.1	−2.9 ± 5.1	−6.5 ± 6.0
	SJ (#7) vs. TRM (#8)	4.1 ± 4.5	−1.9 ± 4.5	−5.0 ± 5.2

Note. TH, YL, SJ, and TRM stand for the Turfan-Hami, Yili, South Junggar, and Tarim blocks. Plat ± Δplat and Rot ± Δrot correspond to relative latitudinal displacements and rotations (and the errors) between blocks. The reference numbers #no. of each paleomagnetic pole are consistent with that in Figure 11 and Table S4. The relative movements between the blocks are calculated using an average sampling site at 43.4°N, 90.3°E.

Between the Turpan-Hami and South Junggar blocks, significant relative movements since the Early Permian are suggested by an angular difference of 22.0° ± 7.2° between their Early Permian paleomagnetic poles. Such discordance can be explained by a clockwise relative rotation of 21.2° ± 9.4° and northward latitudinal movement of 14.7° ± 7.2° of the Turpan-Hami Block with respect to the South Junggar Block since the Early Permian. According to previous paleomagnetic studies (Choulet et al., 2011; Zhu et al., 2018), large relative rotation corresponding to a dextral displacement of 630 ± 295 km along the NTF occurred between the Yili and South Junggar blocks after the Late Permian. Considering the aforementioned possibly similar kinematic evolution between the Turpan-Hami and Yili blocks, the clockwise rotation of the Turpan-Hami Block with respect to the South Junggar Block may also reflect large-scale lateral displacement between two blocks along the NTF. The latitudinal movement of 14.7° ± 7.2° between the Turpan-Hami and South Junggar blocks possibly sheds light on a late Paleozoic intra-arc basin in the Bogda Belt and is discussed below.

6.4. Tectonic Implications for a Late Paleozoic Intra-Arc Basin in the Bogda Belt

Being located between the Turpan-Hami and South Junggar blocks, the Bogda Belt experienced Early Permian marine volcanism and sedimentation, Late Permian to Triassic terrigenous deposition, Cretaceous uplift, and Cenozoic shortening (Carroll et al., 1995; Chen et al., 2015; Greene et al., 2001, 2005; Hendrix et al., 1992; Shu et al., 2011; Wartes et al., 2002; Xie et al., 2016). Thus, pulses of late Paleozoic to Cenozoic significant crustal uplift and related shortening may account for the latitudinal movement since the Early Permian between the Turpan-Hami and South Junggar blocks. Numerous studies have estimated the magnitude of N-S shortening since the Cretaceous across the Tianshan Belt. Cenozoic crustal deformation in the western Chinese Tianshan Belt corresponds to ~150 km shortening between the Tarim and Junggar basins (Avouac et al., 1993; Avouac & Tapponnier, 1993). Facies analysis of the Tadjik basin indicates a total crustal shortening of 300 km within the Tianshan and Pamir ranges (Burtman, 2000). In addition, Chen et al. (1991) proposed that the crustal shortening between the Junggar and Tarim blocks since the Cretaceous is 150–175 km in the eastern part of the Tianshan Range and reaches ~280 km in its western part (Kashgar). These conclusions are generally in agreement with each other and also consistent with our estimates based on integrated Cretaceous paleomagnetic results that show estimated relative latitudinal movements of 1.0–2.9° since the Cretaceous (Figure 11b and Table 2). Clearly, these values are much smaller than the total relative latitudinal movements since the Early Permian, which should, therefore, be the result of Early Permian to Cretaceous tectonism.

Greene et al. (2001, 2005) argued for an Early Jurassic initial uplift of the Bogda Belt based on petrographic approaches and trace-element and isotopic geochemistry, which are also supported by paleocurrent, sedimentary facies, and other stratigraphic evidence (Hendrix et al., 1992; Wartes et al., 2002). Unconformities and evolution of sedimentary compositions in the Turpan-Hami basin both suggest a continuous uplift and erosion of the Bogda Belt in the Mesozoic (Greene et al., 2001). Though the Mesozoic uplift of the Bogda Belt may contribute to the crustal shortening, its magnitude is difficult to quantitatively evaluate due to the insufficiency of data. Mesozoic paleomagnetic poles of the Turpan-Hami and Junggar blocks are therefore badly needed to assess this issue. Nevertheless, a preliminary estimate could be carried out based on Early Triassic paleomagnetic poles of South Junggar (Choulet et al., 2013) and Tarim (Zhu et al., 1998). Relative latitudinal movement between the South Junggar and Tarim blocks since the Early Triassic is accordingly approximated as 5.0° ± 12.2°. In paleomagnetism, when uncertainty is large, the calculated value generally provides nothing more than rough qualitative information. Therefore, several hundred kilometers of crustal shortening should have occurred between these two blocks since the Early Triassic. Furthermore, the crustal shortening that took place in the Triassic and Jurassic might be of similar or smaller magnitude than that which occurred since the Cretaceous, as the great India-Eurasia collision began in the Cenozoic. Consequently, the crustal shortening of 300–350 km between South Junggar and Tarim blocks and smaller (~300 km) between South Junggar and Turpan-Hami blocks since the Early Triassic is permitted. The abovementioned crustal shortening between the Turpan-Hami and South Junggar blocks is still much smaller than our estimate of 1,630 ± 800 km (14.7° ± 7.2°) since the Early Permian. Therefore, pre-Triassic tectonic event(s) should also be included in this important crustal shortening.

The late Paleozoic tectonic evolution of the Bogda Belt has been extensively studied, mainly based on geochemistry and geochronology of magmatic rocks. Different tectonic settings have been proposed, such as an island arc (Carroll et al., 1995; Xie et al., 2016), a continental rift (Shu et al., 2011; Xia et al., 2008, 2012), a mantle plume-related large igneous province (Su et al., 2011; Xia et al., 2008), and a postcollision extensional belt (Chen et al., 2011; Ma et al., 2015). Recently, Zhang et al. (2017) suggested that upper Carboniferous volcanic rocks in the Dashitou area from the eastern Bogda Belt formed in an extensional regime associated with a subduction-related environment and proposed an intra-arc rifting tectonic setting. Wali et al. (2018) compiled literature data and suggested that the Carboniferous to Early Permian magmatic rocks in the Bogda Belt generally show consistent arc-type features with increasing mantle input through time, consistent with upwelling of asthenospheric mantle under an intra-arc rifting or pull-apart extension in suprasubduction zone (Branquet et al., 2012; Wang et al., 2009). In addition, Shu et al. (2011) reported an Early Permian deepening sedimentary environment in the Baiyanggou section, southwest of the Bogda Belt, characterized by olistostrome, chert-bearing turbidite, and bimodal volcanic rocks including pillow basalts, likely caused by initiation of intra-arc rifting. The felsic volcanic rocks yield zircon U-Pb ages of 311–297 Ma (Shu et al., 2011; Xie et al., 2016). Therefore, an intra-arc rift basin likely existed in the Bogda Belt during late Carboniferous to early Permian times. The closure of this intra-arc rift basin was poorly constrained as no typical subduction or collision-related records were recognized. However, several lines of evidence indicate important crustal uplift and shortening posterior to the Early Permian. These arguments include (1) a regional unconformity of upper Permian with a thick molasse sequence, (2) a change of sedimentary environments from marine to terrigenous, and (3) tight folds and intense schistosity of the Carboniferous to Lower Permian metasedimentary rocks in the Bogda area (Shu et al., 2011; Wali et al., 2018; XBGMR, 1993). Therefore, we propose that the Bogda intra-arc rift basin was likely closed during the Middle to Late Permian time.

Obviously, the closure of this intra-arc basin should be another important contribution to the relative latitudinal movement between the Turpan-Hami and South Junggar blocks since the Early Permian. Keeping the large uncertainties in mind, by subtracting the maximum estimated amount of crustal shortening between these two blocks since the Early Triassic (~300 km), a northward movement of at least 530 km for the Turpan-Hami Block with respect to South Junggar could be proposed, which resulted from the closure of the intra-arc rift basin in the Bogda Belt. Clearly, more paleomagnetic studies and further geologic investigations are needed to verify this hypothesis.

7. Conclusions

1. The first Early Permian paleomagnetic pole for the Turpan-Hami Block is obtained from Lower Permian sedimentary rocks at $\lambda = 75.7°$N, $\varphi = 276.3°$E, $A_{95} = 5.7°$, and $N = 10$ sites.
2. The Turpan-Hami and Yili blocks have maintained their relative position since the Early Permian and likely experienced a similar kinematic evolution since then with respect to their surrounding blocks.
3. The Turpan-Hami Block experienced relative rotations of $-41.1° \pm 7.1°$ and $21.2° \pm 9.4°$ with respect to the Tarim and South Junggar blocks since the Early Permian, respectively. This corresponds to large-magnitude strike-slip movements along major strike-slip faults which characterize the main intracontinental tectonic features of the SW CAOB since the late Paleozoic.
4. Small but significant latitudinal movements of $8.3° \pm 5.9°$ and $14.7° \pm 7.2°$ are revealed for the Turpan-Hami Block with respect to the Tarim and South Junggar blocks, respectively. The former could be interpreted as the result of a strike-slip displacement along the NE-SW-striking Nalati Fault-MTSZ, instead of crustal shortening. The latter was possibly accommodated by the closure of a ~530 km-width intra-arc rift basin that existed between the South Junggar and Turpan-Hami blocks in the Early Permian and by subsequent uplifts of the Bogda Range.

Acknowledgments
We thank Ms. Xuzhi Hu and Dr. Yongxiang Li for providing laboratory guidance. We also appreciate Mrs. Pan Liu, Xiaozhan Li, and Kang Shuai for their kind help in the laboratory analyses. Prof. John Geissman and another anonymous reviewer together with the editors are very much thanked for their constructive comments and suggestions. This study was cosponsored by the National Natural Science Foundation of China (41772225, 41390445, 41172197, and 41222019) and by the Open Fund of State Key Laboratory for Mineral Deposits Research (ZZKT-201603). The support provided by China Scholarship Council (CSC, 201806190163) and labex VOLTAIRE (ANR-10-LABX-100-01) is appreciated for financing part of research of the first author in France. Our data of this study can be downloaded from the figshare website (doi: 10.6084/m9.figshare.10099358).

References

Allen, M. B., Windley, B. F., & Zhang, C. (1993). Palaeozoic collisional tectonics and magmatism of the Chinese tien Shan, Central Asia. *Tectonophysics*, *220*(1-4), 89–115. https://doi.org/10.1016/0040-1951(93)90225-9

Andersen, T. (2002). Correction of common lead in U–Pb analyses that do not report ^{204}Pb. *Chemical Geology*, *192*(1-2), 59–79. https://doi.org/10.1016/S0009-2541(02)00195-X

Avouac, J. P., & Tapponnier, P. (1993). Kinematic model of active deformation in Central Asia. *Geophysical Research Letters*, *20*(10), 895–898. https://doi.org/10.1029/93GL00128

Avouac, J. P., Tapponnier, P., Bai, M., You, H., & Wang, G. (1993). Active thrusting and folding along the northern tien Shan and late Cenozoic rotation of the Tarim relative to Dzungaria and Kazakhstan. *Journal of Geophysical Research Solid Earth*, *98*(B4), 6755–6804. https://doi.org/10.1029/92JB01963

Bai, Y. H., Chen, G. L., Sun, Q. G., Sun, Y. H., Li, Y. G., Dong, Y. J., & Sun, D. J. (1987). Late Paleozoic polar wander path for the Tarim platform and its tectonic significance. *Tectonophysics*, *139*(1-2), 145–153. https://doi.org/10.1016/0040-1951(87)90203-4

Belica, M. E., Tohver, E., Pisarevsky, S. A., Jourdan, F., Denyszyn, S., & George, A. D. (2017). Middle Permian paleomagnetism of the Sydney Basin, eastern Gondwana: Testing Pangea models and the timing of the end of the Kiaman reverse Superchron. *Tectonophysics*, *699*, 178–198. https://doi.org/10.1016/j.tecto.2016.12.029

Black, L. P., & Gulson, B. L. (1978). The age of the mud tank carbonatite, Strangways range, Northern Territory. *BMR Journal of Australian Geology and Geophysics*, *3*(3), 227–232.

Branquet, Y., Gumiaux, C., Sizaret, S., Barbanson, L., Wang, B., Cluzel, D., et al. (2012). Synkinematic mafic/ultramafic sheeted intrusions: Emplacement mechanism and strain restoration of the Permian Huangshan Ni–cu ore belt (eastern Tianshan, NW China). *Journal of Asian Earth Sciences*, *56*, 240–257. https://doi.org/10.1016/j.jseaes.2012.05.021

Burtman, V. S. (2000). Cenozoic crustal shortening between the Pamir and tien Shan and a reconstruction of the Pamir–tien Shan transition zone for the cretaceous and Paleogene. *Tectonophysics*, *319*(2), 69–92. https://doi.org/10.1016/S0040-1951(00)00022-6

Butler, R. F. (1992). *Paleomagnetism: Magnetic Domains to Geologic Terranes*. Boston: Blackwell Scientific.

Carroll, A. R., Graham, S. A., Hendrix, M. S., Ying, D., & Zhou, D. (1995). Late Paleozoic tectonic amalgamation of northwestern China: Sedimentary record of the northern Tarim, northwestern Turpan, and southern Junggar Basins. *American Journal of Science*, *107*(5), 571–594. https://doi.org/10.1130/0016-7606(1995)107<0571:LPTAON>2.3.CO;2

Chen, K., Lin, W., & Wang, Q. (2015). The Bogeda Shan uplifting: Evidence from multiple phases of deformation. *Journal of Asian Earth Sciences*, *99*, 1–12. https://doi.org/10.1016/j.jseaes.2014.12.006

Chen, X. J., Shu, L. S., & Santosh, M. (2011). Late Paleozoic post-collisional magmatism in the eastern Tianshan belt, Northwest China: New insights from geochemistry, geochronology and petrology of bimodal volcanic rocks. *Lithos*, *127*(3-4), 581–598. https://doi.org/10.1016/j.lithos.2011.06.008

Chen, Y., Cogné, J. P., & Courtillot, V. (1992). New cretaceous paleomagnetic poles from the Tarim basin, northwestern China. *Earth and Planetary Science Letters*, *114*(1), 17–38. https://doi.org/10.1016/0012-821X(92)90149-P

Chen, Y., Cogné, J. P., Courtillot, V., Avouac, J. P., Tapponnier, P., Wang, G. Q., et al. (1991). Paleomagnetic study of Mesozoic continental sediments along the Northern Tien Shan (China) and heterogeneous strain in Central Asia. *Journal of Geophysical Research-Solid Earth*, *96*(B3), 4065–4082. https://doi.org/10.1029/90JB026990148-0227/91/90JB-02699$05.00

Choulet, F., Chen, Y., Cogné, J. P., Rabillard, A., Wang, B., Lin, W., et al. (2013). First Triassic palaeomagnetic constraints from Junggar (NW China) and their implications for the Mesozoic tectonics in Central Asia. *Journal of Asian Earth Sciences*, *78*(12), 371–394. https://doi.org/10.1016/j.jseaes.2013.01.023

Choulet, F., Chen, Y., Wang, B., Faure, M., Cluzel, D., Charvet, J., et al. (2011). Late Paleozoic paleogeographic reconstruction of Western Central Asia based upon paleomagnetic data and its geodynamic implications. *Journal of Asian Earth Sciences*, *42*(5), 867–884. https://doi.org/10.1016/j.jseaes.2010.07.011

Choulet, F., Faure, M., Cluzel, D., Chen, Y., Lin, W., & Wang, B. (2012). From oblique accretion to transpression in the evolution of the Altaid collage: New insights from west Junggar, northwestern China. *Gondwana Research*, *21*(2-3), 530–547. https://doi.org/10.1016/j.gr.2011.07.015

Cogné, J. P. (2003). PaleoMac: A Macintosh™ application for treating paleomagnetic data and making plate reconstructions. *Geochemistry, Geophysics, Geosystems*, *4*(1), 1007. https://doi.org/10.1029/2001GC000227

Cogné, J. P., Chen, Y., Courtillot, V., Rocher, F., Wang, G., Bai, M., & You, H. (1995). A paleomagnetic study of Mesozoic sediments from the Junggar and Turfan basins, northwestern China. *Earth and Planetary Science Letters*, *133*(3–4), 353–366. https://doi.org/10.1016/0012-821X(95)00083-O

Deenen, M. H. L., Langereis, C. G., Van Hinsbergen, D. J. J., & Biggin, A. J. (2011). Geomagnetic secular variation and the statistics of palaeomagnetic directions. *Geophysical Journal International*, *186*(2), 509–520. https://doi.org/10.1111/j.1365-246X.2011.05050.x

Dunlop, D. J., Özdemir, Ö., & Schmidt, P. W. (1997). Paleomagnetism and paleothermometry of the Sydney Basin 2. Origin of anomalously high unblocking temperatures. *Journal of Geophysical Research - Solid Earth*, *102*(B12), 27,285–27,295. https://doi.org/10.1029/97jb02478

Fang, D. J., Chen, H. L., Wang, P. Y., & Tan, X. D. (1997). Paleomagnetic study of its tectonic significance for Tarim Basin in Mesozoic. *Chinese Journal of Geophysics*, *40*(1), 47–55. (in Chinese with English abstract)

Fang, D. J., Jin, G. H., Jiang, L. P., Wang, P. Y., & Wang, Z. L. (1996). Paleozoic paleomagnetic results and the tectonic significance of Tarim plate. *Chinese Journal of Geophysics*, *39*(4), 522–532. (in Chinese with English abstract)

Fang, D. J., Shen, Z. Y., & Tan, X. D. (2001). Paleomagnetic study on Kuche depression of Tarim block in early cretaceous and its inclination shallowing. *Chinese Journal of Geophysics*, *44*(1), 72–82. (in Chinese with English abstract)

Fisher, R. (1953). Dispersion on a sphere. *Proceedings of the Royal Society of London*, *217*(1130), 295–305. https://doi.org/10.1098/rspa.1953.0064

Gao, J., Li, M., Xiao, X., Tang, Y., & He, G. (1998). Paleozoic tectonic evolution of the Tianshan Orogen, northwestern China. *Tectonophysics*, *287*(1-4), 213–231. https://doi.org/10.1016/S0040-1951(98)80070-X

Geng, H. Y., Sun, M., Yuan, C., Xiao, W. J., Xian, W. S., Zhao, G. C., et al. (2009). Geochemical, Sr-Nd and zircon U-Pb-Hf isotopic studies of late carboniferous magmatism in the west Junggar, Xinjiang: Implications for ridge subduction? *Chemical Geology*, *266*(3-4), 364–389. https://doi.org/10.1016/j.chemgeo.2009.07.001

Gilder, S., Chen, Y., Cogné, J. P., Tan, X. D., Courtillot, V., Sun, D. J., & Li, Y. G. (2003). Paleomagnetism of upper Jurassic to lower cretaceous volcanic and sedimentary rocks from the western Tarim Basin and implications for inclination shallowing and absolute dating of the M-0 (ISEA?) chron. *Earth and Planetary Science Letters*, *206*(3-4), 587–600. https://doi.org/10.1016/S0012-821X(02)01074-9

Greene, T. J., Carroll, A. R., Hendrix, M. S., Graham, S. A., Wartes, M. A., & Abbink, O. A. (2001). Sedimentary record of Mesozoic deformation and inception of the Turpan-Hami basin, Northwest China. *Geological Society of America Memoirs*, 317–340. https://doi.org/10.1130/0-8137-1194-0.317

Greene, T. J., Carroll, A. R., Wartes, M., Graham, S. A., & Wooden, J. L. (2005). Integrated provenance analysis of a complex orogenic terrane: Mesozoic uplift of the Bogda Shan and inception of the Turpan-Hami basin, NW China. *Journal of Sedimentary Research*, *75*(2), 251–267. https://doi.org/10.2110/jsr.2005.019

Han, B. F., He, G. Q., Wang, X. C., & Guo, Z. J. (2011). Late carboniferous collision between the Tarim and Kazakhstan–Yili terranes in the western segment of the South Tian Shan Orogen, Central Asia, and implications for the northern Xinjiang, western China. *Earth-Science Reviews*, *109*(3-4), 74–93. https://doi.org/10.1016/j.earscirev.2011.09.001

Hendrix, M. S., Graham, S. A., Carroll, A. R., Sobel, E. R., Mcknight, C. L., Schulein, B. J., & Wang, Z. (1992). Sedimentary record and climatic implications of recurrent deformation in the Tian Shan: Evidence from Mesozoic strata of the North Tarim, south Junggar, and Turpan basins, Northwest China. *Geological Society of America Bulletin*, *104*(1), 53–79. https://doi.org/10.1130/0016-7606(1992)104<0053:SRACIO>2.3.CO;2

Huang, B. C., Wang, Y. C., Liu, T., Yang, T. S., Li, Y. A., Sun, D. J., & Zhu, R. X. (2004). Paleomagnetism of Miocene sediments from the Turfan basin, Northwest China: No significant vertical-axis rotation during Neotectonic compression within the Tian Shan range, Central Asia. *Tectonophysics*, *384*(1-4), 1–21. https://doi.org/10.1016/j.tecto.2004.01.003

Huang, B. C., Wang, Y. C., & Zhu, R. X. (2004). New paleomagnetic and magnetic fabric results for early cretaceous rocks from the Turpan intramontane basin, East Tianshan, Northwest China. *Science in China*, *47*(6), 540–550. https://doi.org/10.1360/02yd0132

Huang, W., Van Hinsbergen, D. J. J., Maffione, M., Orme, D. A., Dupont-Nivet, G., Guilmette, C., et al. (2015). Lower cretaceous Xigaze ophiolites formed in the Gangdese forearc: Evidence from paleomagnetism, sediment provenance, and stratigraphy. *Earth and Planetary Science Letters*, *415*, 142–153. https://doi.org/10.1016/j.epsl.2015.01.032

Jackson, M. J., Banerjee, S. K., Marvin, J. A., Lu, R., & Gruber, W. (1991). Detrital remanence, inclination errors, and anhysteretic remanence anisotropy: Quantitative model and experimental results. *Geophysical Journal International*, *104*(1), 95–103. https://doi.org/10.1111/j.1365-246X.1991.tb02496.x

Jackson, S. E., Pearson, N. J., Griffin, W. L., & Belousova, E. A. (2004). The application of laser ablation-inductively coupled plasma-mass spectrometry to in situ U–Pb zircon geochronology. *Chemical Geology*, *211*(1–2), 47–69. https://doi.org/10.1016/j.chemgeo.2004.06.017

Jahn, B. M. (2004). The central Asian Orogenic Belt and growth of the continental crust in the Phanerozoic. *Geological Society London Special Publications*, *226*(1), 73–100. https://doi.org/10.1144/GSL.SP.2004.226.01.05

de Jong, K., Wang, B., Faure, M., Shu, L., Cluzel, D., Charvet, J., et al. (2009). New $^{40}Ar/^{39}Ar$ age constraints on the Late Palaeozoic tectonic evolution of the western Tianshan (Xinjiang, northwestern China), with emphasis on Permian fluid ingress. *International Journal of Earth Sciences*, *98*(6), 1239–1258. https://doi.org/10.1007/s00531-008-0338-8

Kirschvink, J. L. (1980). The least squares line and the analysis of paleomagnetic data. *Geophysical Journal International*, *62*(3), 699–718. https://doi.org/10.1111/j.1365-246X.1980.tb02601.x

Kodama, K. P. (2009). Simplification of the anisotropy-based inclination correction technique for magnetite- and haematite-bearing rocks: A case study for the carboniferous Glenshaw and Mauch chunk formations, North America. *Geophysical Journal International*, *176*(2), 467–477. https://doi.org/10.1111/j.1365-246X.2008.04013.x

Kodama, K. P. (2012). *Paleomagnetism of Sedimentary Rocks: Process and Interpretation*. Oxford: Wiley-Blackwel. https://doi.org/10.1002/9781118384138

Koymans, M. R., Langereis, C. G., Pastor-Galán, D., & Hinsbergen, D. J. J. V. (2016). Paleomagnetism.org: An online multi-platform open source environment for paleomagnetic data analysis. *Computers & Geosciences*, *93*, 127–137. https://doi.org/10.1016/j.cageo.2016.05.007

Laurent-Charvet, S., Charvet, J., Monié, P., & Shu, L. (2003). Late Paleozoic strike-slip shear zones in eastern Central Asia (NW China): New structural and geochronological data. *Tectonics*, *22*(2), n/a. https://doi.org/10.1029/2001tc901047

Laurent-Charvet, S., Charvet, J., Shu, L., Ma, R., & Lu, H. (2002). Palaeozoic late collisional strike-slip deformations in Tianshan and Altay, Eastern Xinjiang, NW China. *Terra Nova*, *14*(4), 249–256. https://doi.org/10.1046/j.1365-3121.2002.00417.x

Li, Y. A., Li, Q., Zhang, H., Sun, D. J., Cao, Y., & Wu, S. Z. (1995). Paleomagnetic study of Tarim and its adjacent area as well as the formation and evolution of the basin. *Xinjiang Geology*, *13*(4), 293–378. (in Chinese with English abstract)

Li, Y. P., Sharps, R., Mcwilliams, M., Li, Y., Li, Q., & Zhang, W. (1991). Late Paleozoic paleomagnetic results from the Junggar block, northwestern China. *Journal of Geophysical Research*, *96*(B10), 16047–16060. https://doi.org/10.1029/91JB01619

Li, Y. P., Zhang, Z. K., McWilliams, M., Sharps, R., Zhai, Y. J., Li, Y. A., et al. (1988). Mesozoic paleomagnetic results of the Tarim Craton: Tertiary relative motion between China and Siberia. *Geophysical Research Letters*, *15*(3), 217–220. https://doi.org/10.1029/GL015i003p00217

Ludwig, K. R. (2001). *Squid 1.02: A user manual*. Berkeley: Berkeley Geochronological Center, special publication 2. 19 pp.

Ma, X. X., Shu, L. S., & Meert, J. G. (2015). Early Permian slab breakoff in the Chinese Tianshan belt inferred from the post-collisional granitoids. *Gondwana Research*, *27*(1), 228–243. https://doi.org/10.1016/j.gr.2013.09.018

McElhinny, M. W. (1964). Statistical significance of the fold test in palaeomagnetism. *Geophysical Journal International*, *8*(3), 338–340. https://doi.org/10.1111/j.1365-246X.1964.tb06300.x

Meng, Z. F., Deng, Y. S., Ding, Z. H., Zheng, Y. P., Li, Y. A., & Sun, D. J. (1998). New paleomagnetic results from Ceno-Mesozoic volcanic rocks along southern rim of the Tarim Basin, China. *Science in China*, *41*(Supp), 91–104.

Molnar, P., & Tapponnier, P. (1975). Cenozoic tectonics of Asia: Effects of a continental collision: Features of recent continental tectonics in Asia can be interpreted as results of the India-Eurasia collision. *Science*, *189*(4201), 419–426. https://doi.org/10.1126/science.189.4201.419

Nie, S. Y., Rowley, D. B., Van der Voo, R., & Li, M. S. (1993). Paleomagnetism of late Paleozoic rocks in the Tianshan, northwestern China. *Tectonics*, *12*(2), 568–579. https://doi.org/10.1029/92TC00657

Roberts, A. P., Chang, L., Rowan, C. J., Horng, C. S., & Florindo, F. (2011). Magnetic properties of sedimentary greigite (Fe_3S_4): An update. *Reviews of Geophysics*, *49*, RG1002. https://doi.org/10.1029/2010rg000336

Roberts, A. P., Cui, Y., & Verosub, K. L. (1995). Wasp-waisted hysteresis loops: Mineral magnetic characteristics and discrimination of components in mixed magnetic systems. *Journal of Geophysical Research Solid Earth*, *100*(B9), 17909–17924. https://doi.org/10.1029/95JB00672

Sengör, A. M. C., Natal'in, B. A., & Burtman, V. S. (1993). Evolution of the Altaid tectonic collage and Palaeozoic crustal growth in Eurasia. *Nature*, *364*(6435), 299–307. https://doi.org/10.1038/364299a0

Sharps, R., Li, Y. P., McWilliams, M., & Li, Y. G. (1992). Paleomagnetic investigation of upper Permian sediments in the south Junggar Basin, China. *Journal of Geophysical Research*, *97*(B2), 1753–1765. https://doi.org/10.1029/91JB02741

Sharps, R., Mcwilliams, M., Li, Y., Cox, A., Zhang, Z., Zhai, Y., et al. (1989). Lower Permian paleomagnetism of the Tarim block, northwestern China. *Earth and Planetary Science Letters*, *92*(3–4), 275–291. https://doi.org/10.1016/0012-821X(89)90052-6

Shu, L., Wang, B., Zhu, W., Guo, Z., Charvet, J., & Zhang, Y. (2011). Timing of initiation of extension in the Tianshan, based on structural, geochemical and geochronological analyses of bimodal volcanism and olistostrome in the Bogda Shan (NW China). *International Journal of Earth Sciences*, *100*(7), 1647–1663. https://doi.org/10.1007/s00531-010-0575-5

Shu, L., Yu, J., Charvet, J., Laurent-Charvet, S., Sang, H., & Zhang, R. (2004). Geological, geochronological and geochemical features of granulites in the eastern Tianshan, NW China. *Journal of Asian Earth Sciences*, *24*(1), 25–41. https://doi.org/10.1016/j.jseaes.2003.07.002

Su, B. X., Qin, K. Z., Sakyi, P. A., Li, X. H., Yang, Y. H., Sun, H., et al. (2011). U–Pb ages and Hf–O isotopes of zircons from late Paleozoic mafic–ultramafic units in the southern central Asian Orogenic Belt: Tectonic implications and evidence for an early-Permian mantle plume. *Gondwana Research*, *20*(2–3), 516–531. https://doi.org/10.1016/j.gr.2010.11.015

Tan, X., & Kodama, K. P. (2003). An analytical solution for correcting palaeomagnetic inclination error. *Geophysical Journal International*, *152*(1), 228–236. https://doi.org/10.1046/j.1365-246X.2003.01848.x

Tarling, D., & Hrouda, F. (1993). *Magnetic Anisotropy of Rocks*. London: Chapman & Hall.

Tauxe, L., Butler, R. F., Van der Voo, R., & Banerjee, S. K. (2010). *Essentials of Paleomagnetism*. Berkeley: University of California Press.

Tauxe, L., & Kent, D. V. (2004). A simplified statistical model for the geomagnetic field and the detection of shallow bias in paleomagnetic inclinations: Was the ancient magnetic field dipolar?. In J. E. T. Channell et al. (Eds.).*Timescales of the Paleomagnetic Field*, *Geophysical Monograph Series* (Vol. 145, pp. 101–115). Washington, DC: AGU.

Tauxe, L., Kodama, K. P., & Kent, D. V. (2008). Testing corrections for paleomagnetic inclination error in sedimentary rocks: A comparative approach. *Physics of the Earth and Planetary Interiors*, *169*(1-4), 152–165. https://doi.org/10.1016/j.pepi.2008.05.006

Tauxe, L., & Watson, G. S. (1994). The fold test: An eigen analysis approach. *Earth and Planetary Science Letters*, *122*(3-4), 331–341. https://doi.org/10.1016/0012-821X(94)90006-X

Thébault, E., Finlay, C. C., Beggan, C. D., Alken, P., Aubert, J., Barrois, O., et al. (2015). International geomagnetic reference field: The 12th generation. *Earth, Planets and Space*, *67*(1), 79. https://doi.org/10.1186/s40623-015-0228-9

Wali, G., Wang, B., Cluzel, D., & Zhong, L. (2018). Carboniferous–Early Permian magmatic evolution of the Bogda Range (Xinjiang, NW China): Implications for the Late Paleozoic accretionary tectonics of the SW Central Asian Orogenic Belt. *Journal of Asian Earth Sciences*, *153*, 238–251. https://doi.org/10.1016/j.jseaes.2017.07.045

Wang, B., Chen, Y., Zhan, S., Shu, L., Faure, M., Cluzel, D., et al. (2007). Primary Carboniferous and Permian paleomagnetic results from the Yili Block (NW China) and their implications on the geodynamic evolution of Chinese Tianshan Belt. *Earth and Planetary Science Letters*, *263*(3-4), 288–308. https://doi.org/10.1016/j.epsl.2007.08.037

Wang, B., Cluzel, D., Jahn, B. M., Shu, L., Chen, Y., Zhai, Y., et al. (2014). Late Paleozoic pre- and syn-kinematic plutons of the Kangguer-Huangshan shear zone; inference on the tectonic evolution of the eastern Chinese north Tianshan. *American Journal of Science*, *314*(1), 43–79. https://doi.org/10.2475/01.2014.02

Wang, B., Cluzel, D., Shu, L., Faure, M., Charvet, J., Chen, Y., et al. (2009). Evolution of calc-alkaline to alkaline magmatism through carboniferous convergence to Permian transcurrent tectonics, western Chinese Tianshan. *International Journal of Earth Sciences*, *98*(6), 1275–1298. https://doi.org/10.1007/s00531-008-0408-y

Wang, B., Faure, M., Cluzel, D., Shu, L. S., Charvet, J., Meffre, S., & Ma, Q. (2006). Late Paleozoic tectonic evolution of the northern west Chinese Tianshan Belt. *Geodinamica Acta*, *19*(3–4), 237–247. https://doi.org/10.3166/ga.19.237-247

Wang, B., Faure, M., Shu, L. S., Cluzel, D., Charvet, J., de Jong, K., & Chen, Y. (2008). Paleozoic geodynamic evolution of the Yili block, western Chinese Tianshan. *Bulletin de la Société Géologique de France*, *179*(5), 483–490. https://doi.org/10.2113/gssgfbull.179.5.483

Wang, B., Zhai, Y., Kapp, P., De Jong, K., Zhong, L., Liu, H., et al. (2018). Accretionary tectonics of back-arc oceanic basins in the south Tianshan: Insights from structural, geochronological, and geochemical studies of the Wuwamen ophiolite mélange. *Geological Society of America Bulletin*, *130*(1-2), 284–306. https://doi.org/10.1130/B31397.1

Wang, Y., Li, J. Y., & Sun, G. H. (2008). Postcollisional eastward extrusion and tectonic exhumation along the eastern Tianshan Orogen, Central Asia: Constraints from dextral strike-slip motion and $^{40}Ar/^{39}Ar$ geochronological evidence. *The Journal of Geology*, *116*(6), 599–618. https://doi.org/10.1086/591993

Wartes, M. A., Carroll, A. R., & Greene, T. J. (2002). Permian sedimentary record of the Turpan-Hami basin and adjacent regions, northwest China: Constraints on postamalgamation tectonic evolution. *Geological Society of America Bulletin*, *114*(2), 131–152. https://doi.org/10.1130/0016-7606(2002)114<0131:PSROTT>2.0.CO;2

Wilhem, C., Windley, B. F., & Stampfli, G. M. (2012). The Altaids of Central Asia: A tectonic and evolutionary innovative review. *Earth-Science Reviews*, *113*(3-4), 303–341. https://doi.org/10.1016/j.earscirev.2012.04.001

Windley, B. F., Alexeiev, D., Xiao, W., Kröner, A., & Badarch, G. (2007). Tectonic models for accretion of the central Asian Orogenic Belt. *Journal of the Geological Society*, *164*(1), 31–47. https://doi.org/10.1144/0016-76492006-022

XBGMR (Xinjiang Bureau of Geology and Mineral Resources) (1960). Geological Map 1:200000, Tuokexun Sheet (L-45-11)

XBGMR (Xinjiang Bureau of Geology and Mineral Resources) (1973). Geological Map 1:200000, Qijiaojing Sheet (L-46-11)

XBGMR (Xinjiang Bureau of Geology and Mineral Resources) (1988). Geological Map 1:200000, Dabancheng Sheet (L-45-5)

XBGMR (Xinjiang Bureau of Geology and Mineral Resources) (1993). *Regional Geology of Xinjiang Uygur Autonomy Region* (pp. 1–841). Beijing: Geology Publishing House. (in Chinese with English abstract)

XGSC (Xi'an Geological Survey Center) (2007). Geological Map of Tianshan and Adjacent region (1:1000000)

Xia, L. Q., Xia, Z. C., Xu, X. Y., Li, X. M., & Ma, Z. P. (2008). Relative contributions of crust and mantle to the generation of the Tianshan carboniferous rift-related basic lavas, northwestern China. *Journal of Asian Earth Sciences*, *31*(4–6), 357–378. https://doi.org/10.1016/j.jseaes.2007.07.002

Xia, L. Q., Xu, X. Y., Li, X. M., Ma, Z. P., & Xia, Z. C. (2012). Reassessment of petrogenesis of carboniferous–early Permian rift-related volcanic rocks in the Chinese Tianshan and its neighboring areas. *Geoscience Frontiers*, *3*(4), 445–471. https://doi.org/10.1016/j.gsf.2011.12.011

Xie, W., Luo, Z. Y., Xu, Y. G., Chen, Y. B., Hong, L. B., Ma, L., & Ma, Q. (2016). Petrogenesis and geochemistry of the late carboniferous rear-arc (or back-arc) pillow basaltic lava in the Bogda Mountains, Chinese north Tianshan. *Lithos*, *244*, 30–42. https://doi.org/10.1016/j.lithos.2015.11.024

Yin, A., & Nie, S. Y. (1996). A Phanerozoic palinspastic reconstruction of China and its neighboring regions. In A. Yin, & M. Harrison (Eds.), *The Tectonic Evolution of Asia*, *Rubey Colloquium* (pp. 442–485). Cambridge: Cambridge University Press.

Yuan, C., Sun, M., Wilde, S., Xiao, W. J., Xu, Y. G., Long, X. P., & Zhao, G. C. (2010). Post-collisional plutons in the Balikun area, east Chinese Tianshan: Evolving magmatism in response to extension and slab break-off. *Lithos*, *119*(3-4), 269–288. https://doi.org/10.1016/j.lithos.2010.07.004

Zhang, Y. Y., Yuan, C., Long, X. P., Sun, M., Huang, Z. Y., Du, L., & Wang, X. Y. (2017). Carboniferous bimodal volcanic rocks in the eastern Tianshan, NW China: Evidence for arc rifting. *Gondwana Research*, *43*, 92–106. https://doi.org/10.1016/j.gr.2016.02.004

Zhao, J., Liu, G., Lu, Z., Zhang, X., & Zhao, G. (2003). Lithospheric structure and dynamic processes of the Tianshan orogenic belt and the Junggar basin. *Tectonophysics*, *376*(3-4), 199–239. https://doi.org/10.1016/j.tecto.2003.07.001

Zhao, P., Chen, Y., Zhan, S., Xu, B., & Faure, M. (2014). The apparent polar wander path of the Tarim block (NW China) since the Neoproterozoic and its implications for a long-term Tarim-Australia connection. *Precambrian Research*, *242*, 39–57. https://doi.org/10.1016/j.precamres.2013.12.009

Zhu, R. X., Yang, Z. Y., Wu, H. N., Ma, X. H., Huang, B. C., Meng, Z. F., & Fang, D. J. (1998). Paleomagnetic constraints on the tectonic history of the major blocks of China during the Phanerozoic. *Science in China*, *41*(2), 1–19. (in Chinese)

Zhu, X., Wang, B., Chen, Y., Liu, H., Horng, C. S., Choulet, F., et al. (2018). First early Permian paleomagnetic pole for the Yili block and its implications for late Paleozoic postorogenic kinematic evolution of the SW central Asian Orogenic Belt. *Tectonics*, *37*(6), 1709–1732. https://doi.org/10.1029/2017TC004642

Zijderveld, J. D. A. (1967). A.C. demagnetization of rocks: Analysis of results. In D. W. Collinson, K. M. Creer, & S. K. Runcorn (Eds.), *Methods on Paleomagnetism* (pp. 245–286). New York: Elsevier.